

**H₂O MASER OBSERVATIONS OF CANDIDATE POST-AGB
STARS
AND
DISCOVERY OF THREE HIGH-VELOCITY WATER
SOURCES**

R. M. Deacon¹

School of Physics A29, University of Sydney, NSW 2006, Australia

R.Deacon@physics.usyd.edu.au

J. M. Chapman

CSIRO Australia Telescope National Facility, P.O. Box 76, Epping, NSW 1710, Australia

A. J. Green

School of Physics A29, University of Sydney, NSW 2006, Australia

M. N. Sevenster

Sterrewacht Leiden, Niels Bohrweg 2, 2333 RA Leiden, The Netherlands

ABSTRACT

We present the results of 22 GHz H₂O maser observations of a sample of 85 post-Asymptotic Giant Branch (post-AGB) candidate stars, selected on the basis of their OH 1612 MHz maser and far-infrared properties. All sources were observed with the Tidbinbilla 70-m radio telescope and 21 detections were made. 86 GHz SiO Mopra observations of a subset of the sample are also presented. Of the 21 H₂O detections, 15 are from sources that are likely to be massive AGB stars and most of these show typical, regular H₂O maser profiles. In contrast, nearly all the detections of more evolved stars exhibited high-velocity H₂O maser emission. Of the five sources seen, v223 (W43A, IRAS 18450–0148) is a well known ‘water-fountain’ source which belongs to a small group of post-AGB stars with highly collimated, high-velocity H₂O maser emission. A second source in our

¹Affiliated with the CSIRO Australia Telescope National Facility

sample, v270 (IRAS 18596+0315), is also known to have high-velocity emission. We report the discovery of similar emission from a further three sources, d46 (IRAS 15445–5449), d62 (IRAS 15544–5332) and b292 (IRAS 18043–2116). The source d46 is an evolved post-AGB star with highly unusual maser properties. The H₂O maser emission from d62 is probably associated with a massive star. The source b292 is a young post-AGB star that is highly likely to be a water-fountain source, with masers detected over a velocity range of 210 km s⁻¹.

Subject headings: masers — stars: AGB and post-AGB — stars: late-type — stars: winds, outflows — planetary nebulae: general — radio lines: stars

1. INTRODUCTION

Planetary nebulae (PN) are seen as the clouds of ionised gas that surround the central cores of dying stars. The nebulae often show beautiful and complex structures: while some appear circular, more than half have elliptical or bipolar shapes, in some cases with complex, filamentary structures (Manchado et al. 2000; Kwok 2000). The cause of the diverse range of PN morphologies is still not well understood but is likely to be associated with rapid changes that occur as a star evolves from the Asymptotic Giant Branch (AGB) to the PN stage.

Most stars with an initial Main Sequence mass below about eight solar masses (M_{\odot}) will evolve to become PN. Towards the end of the AGB stage of stellar evolution, stars lose a significant fraction of their initial mass through pulsation-driven mass loss (Vassiliadis & Wood 1993). The Mira variables are optically-visible long-period variable AGB stars with pulsation periods of $\sim 200 - 800$ days, mass-loss rates of $\sim 10^{-8} - 10^{-6} M_{\odot} \text{ yr}^{-1}$ and envelope expansion velocities of $5 - 10 \text{ km s}^{-1}$. For AGB stars with higher mass-loss rates, the central stars are generally invisible but their circumstellar envelopes can be detected through their infrared and/or radio maser emission (Chapman et al. 1995). The OH/IR stars are AGB stars that extend the properties of Miras with thicker circumstellar envelopes, higher mass-loss rates ($10^{-7} - 10^{-4} M_{\odot} \text{ yr}^{-1}$), longer pulsation periods (300 – 3000 days) and higher expansion velocities ($5 - 30 \text{ km s}^{-1}$). More than 1500 OH/IR stars have been detected from OH maser surveys while far-infrared emission from many thousands of AGB stars has been detected in the InfraRed Astronomical Satellite (IRAS) and Midcourse Space eXperiment (MSX) surveys (van der Veen & Habing 1988; Habing 1996).

In the oxygen-rich circumstellar envelopes of Miras and OH/IR stars, OH, H₂O and SiO maser emission may be detected. The SiO maser emission originates in the upper stellar

atmospheres at heights of several stellar radii while the H₂O maser emission occurs further out, from the warm inner regions of the circumstellar envelopes. The OH 1612 MHz masers occur at even greater distances, in the cooler outer envelopes at typically several hundred stellar radii (Habing 1996). The OH 1612 MHz spectra of OH/IR stars almost invariably show a double-peaked profile consistent with a spherical outflow. For example, 86 per cent of 766 sources detected in an OH 1612 MHz survey of the Galactic Plane have the canonical double-peaked profiles (Sevenster et al. 1997a,b, 2001).

The end of the AGB evolutionary stage probably occurs when so much mass has been lost that a star can no longer support radial pulsations. The mass-loss rate then greatly decreases and the surface temperature of the star rises rapidly. During this ‘post-AGB’ phase, the star changes from losing mass in a slow, dense wind, with a velocity of typically 15 km s⁻¹, to mass loss in a hot, low density wind with a velocity of several hundred km s⁻¹. The hot wind sweeps up and compresses the remnant circumstellar envelope while the central star may again become optically visible as radiation from the star ionises part or all of the remnant envelope (e.g. Kwok et al. 1978). These older post-AGB objects that have become optically visible but are not yet fully-ionised PN are often referred to as ‘proto-planetary nebula’ (PPN).

Several mechanisms have been used to explain the production of non-spherical PN. If the slow AGB wind possesses a weak asymmetry with a dense equatorial region, then a bipolar structure may be produced and amplified during the post-AGB phase by interaction with a fast wind (e.g. Frank & Mellema 1994). Magnetic fields from the stars may also constrain or collimate the stellar winds (e.g. García-Segura et al. 1999). In some cases, bipolarity may also occur due to the presence of companion stars or planets (Wood 2000; Soker 2001).

The hydrodynamical models for interacting stellar winds (ISW) do not predict that strong bipolar structures are formed in the early post-AGB phase, as the central stars are still too cool (< 15 000 K) to produce the fast wind. However, Sahai & Trauger (1998) suggested that fast jets *can* operate in the early post-AGB stage and are the dominant shaping mechanism. The origin of these jets is unclear, although in recent years there has been increasing evidence for high velocity, short-lived jets from post-AGB stars. In some cases the jets are traced by OH or H₂O maser emission or through radio continuum (e.g. Miranda et al. 2001; Imai et al. 2002, 2004; Boboltz & Marvel 2005).

Maser observations provide a powerful tool for identifying and investigating the onset of wind asymmetries during the early post-AGB evolutionary stage. However, to date there have been few systematic studies of the maser properties of post-AGB stars as most studies have concentrated on sources selected to have unusual OH maser properties. We are studying the maser properties of a well-defined sample of 85 candidate post-AGB stars. The sample

was selected from sources likely to be post-AGB stars, based on their far-infrared IRAS and MSX properties (Sevenster 2002a,b), which were detected in an OH 1612 MHz survey of the Galactic Plane with the Australia Telescope Compact Array and Very Large Telescope (hereafter the ATCA/VLA survey, Sevenster et al. 1997a,b, 2001).

In Deacon et al. (2004, hereafter Paper I), the results from single-dish OH 1612, 1665, 1667 and 1720 MHz maser observations were presented. All sources were detected again at 1612 MHz, while 27 sources were measured at 1665 MHz and 47 at 1667 MHz. Twenty five per cent of sources in this sample have maser profiles indicative of aspherical wind morphologies. A possible trend was identified in which some sources with classic peaked OH 1612 MHz spectral profiles evolve into profiles characteristic of developed bipolar outflows.

In this paper, results from single-dish 22 GHz H₂O maser observations for the complete sample are presented. A subset of 11 sources has also been observed at the SiO maser line near 86 GHz and the detections are also reported. The results from a previous radio continuum detection of one source (d46) in 1998 are also discussed.

1.1. H₂O Maser Emission

The 22 GHz maser line comes from the 6₁₆–5₂₃ rotational transition of ortho-H₂O. This transition collisionally inverts over a wide range of conditions: temperatures of several hundred K, abundances $n_{\text{H}_2\text{O}}/n_{\text{H}_2} \sim 2\text{--}4 \times 10^{-4}$ (Cooke & Elitzur 1985) and densities up to $n_{\text{H}_2} \sim 10^{11} \text{ cm}^{-3}$ where collisions thermalise rotational energy levels (Cohen 1989). Model calculations (Cooke & Elitzur 1985) predict that H₂O masers are found between two well-defined radii in the circumstellar envelopes. The outer radius is determined by collision rates that are too low to invert the masing energy levels, and the inner radius by high densities that destroy the inversion through too many collisions. The masing region is predicted to occur at larger radii for stars with higher mass-loss rates, from 10^{14} cm for $\dot{M} = 10^{-7} M_{\odot} \text{ yr}^{-1}$ to $\geq 10^{15} \text{ cm}$ for $\dot{M} = 10^{-5} M_{\odot} \text{ yr}^{-1}$. This model has been confirmed observationally for Miras (Lane et al. 1987; Bains et al. 2003). The dissociation of H₂O by external UV radiation into OH and H is important at radii beyond 10^{15} cm and H₂O maser emission is absent in stars with mass-loss rates below $10^{-8} M_{\odot} \text{ yr}^{-1}$ (Habing 1996).

Very short-period Miras ($P < 200$ days) and semi-regular variables rarely have H₂O masers, due to their low mass-loss rates (Benson & Little-Marenin 1996; Szymczak & Engels 1997). For those Miras and semi-regulars with H₂O masers, the spectra are generally narrow and at velocities close to that of the central star, often in regions where circumstellar material is strongly accelerated outwards and tangential amplification dominates over radial ampli-

cation (Menten & Melnick 1991; Engels & Lewis 1996; Engels et al. 1997). Interferometric observations of Miras and semi-regulars (Chapman et al. 1995; Bains et al. 2003, and references therein) confirm that the H₂O masers are generally located in a thick shell in a radially accelerating region where the envelope expansion velocity increases with increasing distance from the central star. In contrast, OH/IR stars have wider H₂O spectra, often double-peaked and comparable to the OH maser velocity widths (Takaba et al. 1994; Engels & Lewis 1996; Szymczak & Engels 1997). Double-peaked spectra occur from H₂O masers located in regions of the circumstellar envelope where the velocity gradients are small and radial amplification dominates. The velocity separation is also larger in stars with higher mass-loss rates as these stars have larger H₂O maser regions. The blue-shifted peaks are usually stronger than the red-shifted peaks (Takaba et al. 1994; Engels & Lewis 1996), probably due to absorption of red-shifted photons as they pass through the high-density region around the star inside the H₂O maser zone.

In the few previous studies of stellar H₂O masers which included post-AGB stars, a rapid decrease in detection rate was found as stars leave the AGB (Engels & Lewis 1996; Takaba et al. 2001; Valdetaro et al. 2001). Approximately 10–20 post-AGB sources with H₂O maser emission have been detected. In the first study there was evidence for an evolution from double-peaked profiles back to Mira-like single-peaked profiles in older post-AGB stars which still retained H₂O masers. This was considered to be due to decreasing mass-loss rates after the AGB and a consequent switch back to tangential pumping of the H₂O masers. The trend of the blue-shifted features in double-peaked profiles being brighter than the red-shifted features, as in OH/IR stars, is continued in post-AGB stars.

H₂O maser emission has been detected from only two PN; K 3–35 (IRAS 19255+2123, Miranda et al. 2001) and IRAS 17347–3139 (de Gregorio-Monsalvo et al. 2004). In K 3–35 the H₂O masers are located near the central star, probably in the inner part of a rotating and expanding torus, and far from the star at the tips of ~ 800 year old jets that are traced by radio continuum and optical spectral-line emission. In IRAS 17347–3139 they are likely to be in a similar torus close to the central star.

H₂O maser emission has also been detected from five post-AGB stars. In all cases the spectra reveal high-velocity outflows. For four of the five sources high resolution imaging observations have shown high-velocity, collimated jets traced by the H₂O masers. The nature and properties of these ‘water-fountain’ sources are discussed in Section 6.1.

1.2. SiO Maser Emission in Evolved Stars

SiO masers are primarily observed in evolved stars including Miras and OH/IR stars, where they arise from collisionally and/or radiatively pumped rotational levels of excited vibrational states. The transitions most studied are the $v = 1, J = 1-0$ and $v = 2, J = 1-0$ transitions near 43 GHz, and the $v = 1, J = 2-1$ transition near 86 GHz. The SiO masers require column densities of 10^{18} – 10^{19} cm^{-2} and temperatures above ~ 1200 K (Elitzur 1992). There is little correlation between the presence of SiO masers and mass-loss rate or envelope expansion velocity, indicating that these masers form inside the dust condensation radius. Outside the dust condensation radius, most SiO is locked in dust grains and is no longer available for masing transitions.

The SiO maser emission from Mira variables and OH/IR stars is generally seen in ring-like structures (Habing 1996), indicating that they are tangentially amplified in a spherical or quasi-spherical shell. The spectra commonly show a broad peak that is 5–15 km s^{-1} wide and centred on the stellar velocity (Nyman et al. 1998). The emission is highly variable, with lifetimes for individual clumps of no more than a few months seen in both spectral and high-resolution observations (Elitzur 1992; Humphreys 2002). Both infalling and outflow motions have been seen, most notably in multiple observations of the 43 GHz SiO masers around the Mira variable TX Cam made using the Very Long Baseline Array (VLBA) (Diamond & Kemball 2003). The time variability and chaotic velocity field reflect the conditions in the upper atmospheres of these stars.

Detection rates for SiO masers are very low for post-AGB stars. From a large study of SiO maser emission in evolved stars, Nyman et al. (1998) detected only one post-AGB source (at 43 GHz), the bipolar PPN OH 231.8+4.2. This has an unusual double-peaked spectrum with two features separated by 12 km s^{-1} . This source is a candidate binary, with the H_2O and 43 GHz SiO masers associated with a known Mira variable (Gómez & Rodríguez 2001; Sánchez Contreras et al. 2002) and a hotter companion star that may be driving a fast wind that shapes the mass loss from the Mira. The SiO masers may be in a rotating and infalling torus with a radius of 6 AU located around the Mira. IRAS 19312+1950 is another post-AGB SiO maser source with a double-peaked profile at 43 GHz (Nakashima & Deguchi 2000). The peaks are separated by 26 km s^{-1} and a possible interpretation is that the emission comes from a rotating or expanding circumstellar shell.

2. SAMPLE SELECTION

For the OH observations, a complete sample of 88 sources was selected from the ATCA/VLA survey as likely post-AGB sources on the basis of their IRAS and MSX far-infrared colours. Three of the sources (d29, b262, v280) from the initial selection were found to be star-forming regions (Zijlstra et al. 1990, and Paper I) and were not observed at 22 GHz, giving a sample size of 85 in this paper.

Figure 1 plots the sources against their IRAS [12–25], [25–60] and MSX [8–12], [15–21] colours, where $[a-b] = 2.5 \log (S_b/S_a)$, S is the flux density in Jy and a, b , are wavelengths in μm . The sources detected at 22 GHz are plotted with various symbols indicating the different profile types, as described in the caption. The 22 GHz results are discussed in Section 4.

In the IRAS plot the evolutionary path for AGB stars defined by van der Veen & Habing (1988) is shown. The regions associated with more and less massive post-AGB stars respectively are denoted ‘LI’ (Left of IRAS) and ‘RI’ (Right of IRAS) (Sevenster 2002a). The LI sources are associated with the most massive AGB stars, with an average mass of $4 M_\odot$, as determined from their Galactic scale heights (Sevenster 2002b). These stars have very high mass-loss rates and correspondingly high $60 \mu\text{m}$ excesses. van Hoof et al. (1997) found that the LI stars may have an earlier AGB termination than less massive stars, and the stars in the LI region may be at a turn-around point in their evolution before they evolve to redder IRAS [12–25] colours (Sevenster 2002b). From Paper I, LI stars typically have regular OH maser profiles. At 1612 MHz, only 3 out of 30 LI sources have non-regular profiles. They also have a much lower detection rate for OH mainline masers with OH 1667 MHz emission detected from just 14 sources and only one detection at 1665 MHz (Paper I).

The LI region overlaps with the Quad III (AGB) region in the MSX diagram (next paragraph). Coupled with their regular OH profiles and high mass-loss rates, this suggests they may still be AGB stars. The nature of LI sources will be discussed more in Section 5.2.

The RI region encompasses sources with IRAS colours that have traditionally been associated with post-AGB stars, PPN and PN (van der Veen et al. 1989). In comparison with LI sources, the RI sources have an average mass of $1.7 M_\odot$ and lower OH maser outflow velocities (Sevenster 2002b), and more OH mainline emission (Paper I). RI sources also have more irregular OH maser profiles than LI sources (Paper I), indicating they may be more evolved.

The MSX plot is divided into four quadrants. Increasing MSX [8–12] colour was found to accurately indicate evolution of stars off the AGB, and increasing MSX [15–21] colour indicates further post-AGB evolution and possibly the onset of the fast wind (Sevenster

2002a). Thus, older post-AGB stars are found in Quad I, and young post-AGB stars in Quad IV (Sevenster 2002a). The other two quadrants, II and III, contain star-forming regions and AGB stars respectively. The MSX Quad I and IV sources overlap with the IRAS RI region. However, the MSX colours provide better selection criteria for separating younger and older post-AGB sources.

Table 1 lists the 85 sources included in the sample. The first four columns give the source identifier from the ATCA/VLA survey, the IRAS name and the source classifications as RI, LI, Quad I or Quad IV (note some sources have two classifications). The final two columns indicate whether 22 GHz H₂O maser emission and 86 GHz SiO maser emission were detected (y/n). A blank entry in the SiO column indicates the source was not observed. See Sevenster (2002a,b) and Paper I for further details on the selection criteria.

3. OBSERVATIONS

3.1. H₂O Maser Observations

22 GHz observations for all 85 sources were taken as service observations with the Tidbinbilla 70-m radio telescope between 2003 April and 2004 May. The rest frequency assumed is 22.23507985 GHz, which is the weighted average of the three strongest hyperfine components of this transition (Moran et al. 1973). No other hyperfine splitting effects are taken into account. The beam size at 22 GHz is 0.8 arcmin. The bandpass was 16 MHz with 8193 channels, and one circular polarisation (left-hand circular polarisation) was recorded. A four-point position-switching mode was used, with observations east-on-on-west relative to the source position. Offsets were 10 arcmin with 3.5 mins spent at each position, giving 7 mins on-source total. Calibration observations to correct the pointing were performed as necessary, giving an average positional error better than 7 arcsec. Most sources were observed once, excepting d46 and d47, which were observed two and three times respectively. The weak sources d62, d103 and v149 were also observed twice to confirm the detection and the spectra were averaged as they did not change significantly. Table 2 lists the UT dates of observations and the range of system temperatures (T_{sys}) for each date. The system temperatures are elevation and weather dependent.

Initial data reduction to calculate quotient spectra and to average the two on-source observations was carried out using SPC, a single-dish spectral line reduction package supported by the Australia Telescope National Facility (ATNF). Further reduction including velocity, baseline and flux calibration, smoothing and flagging was carried out with the Spectral Line Analysis Package (SLAP; Staveley-Smith 1985). All velocities are given relative to the Local

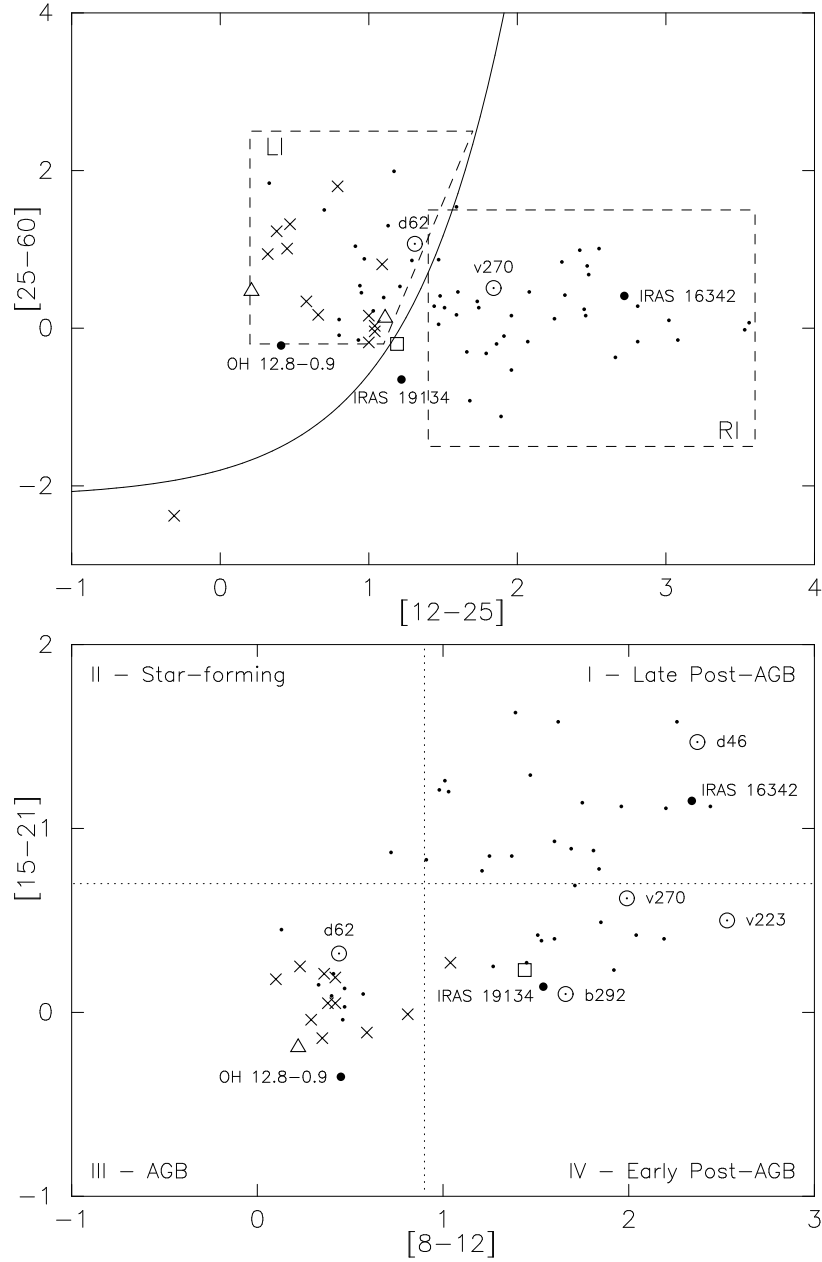


Fig. 1.— IRAS (*top*) and MSX (*bottom*) colour-colour plots of the 85 sources in the post-AGB sample. Sources with no detected H_2O maser emission are indicated with *dots*. Sources with regular spectra (‘R’) are indicated with *crosses*. Those with irregular (‘I’) spectra are marked with *triangles*. The one source with a narrow profile at the stellar velocity (‘S’) is indicated with a *square* and *dotted circles* mark sources with high-velocity features (‘H’). Sources with high-velocity H_2O maser emission are labelled. The three high-velocity sources, IRAS 16342–3814, IRAS 19134+2131 and OH12.8–0.9, that have previously published detections, are shown as *filled circles* (Section 6.1) which are labelled.

Standard of Rest (radio definition).

The 16 MHz bandpass gives a velocity coverage of approximately 200 km s^{-1} and a channel separation of 0.026 km s^{-1} . All spectra were smoothed with a Gaussian function in SLAP to 0.18 km s^{-1} velocity resolution to enable an accurate comparison of spectral features and peak fluxes with the OH maser observations from Paper I. This resulted in rms errors of between 0.04 and $0.13 \text{ Jy beam}^{-1}$ in the final spectra.

3.2. Mopra 86 GHz SiO Observations

A subset of 11 sources (d46, d47, d56, d168, d189, b11, b34, b292, b301, v67, and v117) were observed using the Mopra radio telescope near Coonabarabran, NSW, which is operated jointly by ATNF and the University of New South Wales as a National Facility. Observations were taken in 2004 June and August using a 3-mm SIS receiver system and a 2-bit Australia Telescope correlator as the backend. Spectra were taken at SiO maser line rest frequency 86.243442 GHz . The sources are included in Table 2. Two linear polarisations were used with 1024 channels over a bandwidth of 64 MHz, giving a velocity resolution of 0.22 km s^{-1} . Doppler tracking was implemented. Unfortunately, technical issues and adverse weather, including snow, severely limited the time available for the SiO observations, resulting in a restricted number of sources being measured.

The observations were performed in an ‘on-off’ manner, with the telescope on-source for 1 min followed by a sky observation of the same length. This cycle was repeated 10 times over a 20 min observation. Paddle measurements (where a room-temperature load is driven in front of the receiver) were performed about once an hour to measure the system temperature between observations. However, due to rapidly changing atmospheric conditions and system temperatures, it was not possible to perform reliable amplitude calibrations.

Nearby strong SiO masers were observed once per hour to calibrate the pointing to within 6 arcsec. For the on-source observing time of 10 mins, the system sensitivity (1σ rms) was 90 to 220 mK per channel for T_{sys} measurements ranging from 200 to 500 K. Most sources were observed two or three times and the observations averaged together.

Initial data reduction to calculate quotient spectra, average spectra, and set the velocity scale relative to the Local Standard of Rest was done using SPC. Spectra were then converted to the SLAP format and final plots were made with SLAP. Due to a problem with data headers, the velocities of the SiO spectra are uncertain to within $\pm 1 \text{ km s}^{-1}$.

3.3. Radio Continuum Observations of d46

Radio continuum observations of d46 were taken in November 1998 with the Australia Telescope Compact Array (ATCA) at 3, 6 and 13 cm. The central observing frequencies were 8640, 4800 and 2496 MHz respectively. The observations were taken using the 6D array with a bandwidth of 128 MHz, and a longest baseline of 6 km. At 3 and 6 cm short-track observations were taken with a total observing time of 30 minutes, taken as four cuts of 7–8 minutes. At 13 cm the on-source observing time was 55 mins, taken as 11 cuts over 12 hours. Observations of a secondary calibrator source was taken to correct for atmospheric amplitude and phase variations. The absolute flux scale was determined from observations of PKS B1934–638. The data were reduced using the radio astronomy package Miriad (Sault et al. 1995).

Table 1. Source list with H₂O and SiO maser detections.

ID	IRAS Name	Classification		H ₂ O	SiO
		MSX	IRAS		
d3	14341–6211	Q I	RI	n	...
d34	15338–5202	Q I		n	...
d39	15367–5420		LI	n	...
d46	15445–5449	Q I		y	n
d47	15452–5459		LI	y	y
d56	15514–5323		LI	n	n
d62	15544–5332		LI	y	...
d93	16209–4714		RI	n	...
d103	16314–5018	Q IV		y	...
d117	16372–4808	Q I		n	...
d150	16507–4810		RI	n	...
d168	17004–4119		LI	y	y
d189	17088–4221	Q IV		y	n
b5	17097–3624		RI	n	...
d190	17103–3702		RI	n	...
b11	17150–3224	Q I	RI	n	n
d197	17151–3845	Q I		n	...
b14	17164–3226	Q I	RI	n	...
b15	17162–3751	Q I		n	...
b17	17168–3736	Q IV	RI	n	...
d200	17188–3838		LI	y	...
b25	17193–3546		LI	y	...
b30	17205–3556		LI	n	...
b31	17207–3632		LI	n	...
b33	17227–3623	Q IV		n	...
b34	17230–3348	Q IV	LI	n	n
d202	17245–3951	Q I	RI	n	...
b44	17256–3258		LI	n	...
b62	17293–3302		RI	n	...
b68	17310–3432		RI	n	...
b70	17317–2743		RI	n	...
b96	17359–2902	Q I	RI	n	...

Table 1—Continued

ID	IRAS Name	Classification		H ₂ O	SiO
		MSX	IRAS		
b106	17367–3134	Q I		n	...
b112	17370–3357		RI	n	...
b114	17371–2747		RI	n	...
b128	17385–3332		RI	n	...
b130	17390–2809	Q IV		n	...
b133	17392–3020		LI	y	...
b134	17393–2727		RI	n	...
b143	17404–2713		RI	n	...
b155	17414–3108		LI	n	...
b165	17426–2804		LI	n	...
b199	17461–2741	Q IV		n	...
b209	17479–3032		RI	n	...
b210	17482–2501		RI	n	...
b228	17506–2955		RI	n	...
b246	17543–3102		RI	n	...
b250	17548–2753		RI	n	...
b251	17550–2120	Q IV	RI	n	...
b258	17560–2027		RI	n	...
b263	17576–2653	Q I	RI	n	...
b266	17582–2619	Q I	RI	n	...
b292	18043–2116	Q IV		y	n
b300	18051–2415	Q IV	RI	n	...
b301	18052–2016		LI	y	y
b304	18070–2332	Q IV		n	...
v41	18076–1853	Q I		n	...
v45	18087–1440	Q I	RI	n	...
v50	18092–2347		LI	n	...
v53	18100–1915		LI	n	...
v56	18103–1738		LI	y	...
v67	18135–1456	Q IV	RI	n	n
v87	18182–1504		LI	n	...
v117	18246–1032		RI	n	n

4. RESULTS

From the Tidbinbilla observations, 21 stars from the sample of 85 were detected at 22 GHz. Summary data are shown in Table 3, with the columns indicating:

- 1: Source name as in the ATCA/VLA survey. Repeat observations are designated by bracketed numbers. Sources for which two observations have been averaged are indicated with a superscript ‘a’.
- 2-4: Velocity, peak flux density and integrated flux density for the blue-shifted emission for sources with clearly separated blue- and red-shifted peaks, or for the strongest emission feature for sources with one-sided or irregular spectra.
- 5-7: Velocity, peak flux density and integrated flux density for the red-shifted feature of double-peaked sources.
- 8-9: The most extreme blue and red velocities for which emission was detected.
- 10: H₂O maser profile type. ‘R’ indicates a regular double-peaked spectrum, or a single-peaked spectrum where the single feature is near the most red- or blue-shifted OH peaks or velocity limit. ‘S’ indicates a spectrum with a narrow profile centred near the stellar velocity. ‘I’ indicates an irregular spectrum with many emission features over a velocity range similar to the OH velocity range. ‘H’ indicates a spectrum with features at significantly larger velocities than the OH emission, relative to the central stellar velocity.

Figures 2 to 5 show the Gaussian smoothed spectra for the detections at 22 GHz, including the repeated observations of d46 and d47. The OH 1612 MHz spectra from Paper I are also shown for comparison. Figure 6 shows the H₂O maser spectra of b292 and v223 for the full velocity range observed, revealing the very high-velocity features present in these two sources.

Table 4 gives the number of OH 1612 MHz detections and 22 GHz H₂O detections for each of the four infrared selection groups and for the four spectral profile types R, S, I and H. The columns give, from left to right, the frequency or profile type referred to, the total number of sources detected at that frequency or profile, and the number of RI, LI, Quad I and Quad IV sources detected.

SiO masers at 86 GHz were detected for three sources: d47, d168 and b301. All three are LI sources, from the sample of six LI and five non-LI sources observed. Two of the

Table 1—Continued

ID	IRAS Name	Classification		H ₂ O	SiO
		MSX	IRAS		
v120	18257–1052		LI	n	...
v121	18257–1000		LI	y	...
v132	18276–1431	Q I	RI	n	...
v146	18310–0806	Q I		n	...
v149	18314–0900		LI	y	...
v154	18327–0715		LI	y	...
v162	18342–0655	Q I		n	...
v169	18355–0712		RI	n	...
v172	18361–0647		LI	n	...
v189	18389–0601		LI	n	...
v204	18420–0512	Q I	RI	n	...
v211	18432–0149		LI	n	...
v212	18434–0202		LI	y	...
v223	18450–0148	Q IV		y	...
v228	18460–0254		LI	y	...
v231	18467–0238	Q IV	RI	n	...
v237	18485+0642	Q I	RI	n	...
v239	18488–0107		LI	y	...
v268	18588+0428		LI	y	...
v270	18596+0315	Q IV	RI	y	...
v274	19024+0044	Q I	RI	n	...

Table 2. Schedule of H₂O maser observations

UT date	T_{sys} (K)
Tidbinbilla, 22 GHz	
2003 Apr 23	77
2003 Jul 1	55–90
2003 Aug 28	56
2003 Nov 15	82–100
2004 Feb 27–28	59–122
2004 Mar 4	45–82
2004 Mar 9	51–76
2004 Mar 10	61–81
2004 Mar 11–12	91–182
2004 Mar 16–17	63–119
2004 Apr 14	76
2004 May 16	35–56
2004 May 20	50–60
Mopra, 86 GHz	
2004 June 18	200–500
2004 August 26	200–500

objects (d47 and d168) were detected on each of the observation dates with similar profiles each time. Figure 7 shows the spectra from the average of the two linear polarisations for the detections on 2004 August 26.

Discussion of the individual sources follows, including remarks on the SiO maser detections, previous observations, unusual features and likely blending of components.

4.1. Individual Source Notes

This section gives notes for all sources with 22 GHz H₂O or 86 GHz SiO detections from this study. Notes are also given for sources that were not detected but have been observed in previous 22 GHz H₂O or 43 or 86 GHz SiO studies. Where the observing frequency is not specified, the 22 GHz H₂O maser transition is implied. The central velocity of a spectrum is defined as the velocity mid-way between the most extreme blue and red-shifted emission at a detection level of ~ 3 sigma.

d3: Not detected. Observed at 86 GHz (no detection) by Nyman et al. (1998).

d46: This source has irregular and broad emission at the OH (1612, 1665 and 1667) and 22 GHz H₂O transitions, with maser features present over a velocity range of -200 to -60 km s⁻¹. The three OH profiles are blue-shifted with respect to the H₂O maser profile, with an average of 50 km s⁻¹ difference between the the OH and H₂O central velocities. The spectral profiles and peak and integrated intensities at 22 GHz were similar on 2003 August 28 and November 15, although the peak flux of the strong feature at a velocity of -121 km s⁻¹ decreased substantially between the two epochs. A few weak 22 GHz features detected just off the red-shifted end (up to -34 km s⁻¹) of the 2003 Nov spectrum are not plotted.

d47: This is the only source with a four-peaked ‘DD’ OH 1612 MHz spectral profile (Paper I). 22 GHz observations were taken on 2003 August 28, 2003 November 15 and 2004 May 20. The peak intensity of the brightest features decreased between the first two epochs although the integrated flux density over the spectrum remained constant. By 2004 May most features had dimmed to about half their initial peak intensity and the integrated flux had decreased by around 70 per cent. SiO maser emission at 86 GHz was detected, with two features at approximately -40 and -75 km s⁻¹.

d62: The OH single-dish spectrum for d62 is cut at -68 km s⁻¹ where there is confusion with d59 (Paper I). The stellar velocity, determined from the OH 1612 MHz maser spectrum, is -118 km s⁻¹ (Deacon et al. 2004). The single weak feature at 22 GHz is separated from the stellar velocity by about 45 km s⁻¹, and is well outside the OH 1612 MHz emission. It

Table 3. 22 GHz H₂O maser results

Name	V_{bp} (km s ⁻¹)	S_{bp} (Jy)	I_b (Jy km s ⁻¹)	V_{rp} (km s ⁻¹)	S_{rp} (Jy)	I_r (Jy km s ⁻¹)	V_{bl} (km s ⁻¹)	V_{rl} (km s ⁻¹)	Profile
d46	-121.0	9.3	66	-145	-54	H
(2)	-136.9	9.3	62	-145	-34	-
d47	-41.4	6.3	37	-83	-32	I
(2)	-41.4	5.0	34	-82	-32	-
(3)	-38.3	2.3	11	-82	-33	-
d62 ^a	-73.6	0.9	0.5	-75	-72	H
d103 ^a	-63.6	0.5	0.9	-65	-62	R
d168	-21.7	12.1	30	-25	-16	R
d189	-2.2	46.0	140	-5	16	S
d200	-87.4	0.6	1.1	-59.4	0.4	0.9	-90	-57	R
b25	14.9	0.6	0.3	21.2	1.0	1.5	11	22	R
b133	-16.8	0.3	0.4	15.7	1.3	4.4	-18	21	R
b292	100.2	25.3	51	-20	184	H
b301	26.4	1.9	6.1	14	43	R
v56	-1.7	0.5	1.1	32.5	0.9	2.3	-3	35	R
v121	101.9	0.3	1.1	100	107	R
v149 ^a	20.6	0.3	0.5	19	25	R
v154	29.0	9.3	50	23	66	I
v212	22.9	2.1	4.7	54.2	1.0	3.5	17	59	R
v223	122.7	60.2	190	-60	127	H
v228	85.0	0.4	0.7	83	90	R
v239	63.6	0.6	1.5	60	66	R
v268	32.1	7.6	60	29	74	I
v270	61.6	3.5	5.2	117.8	0.9	0.9	60	119	H

^aSources for which observations at two epochs were averaged together

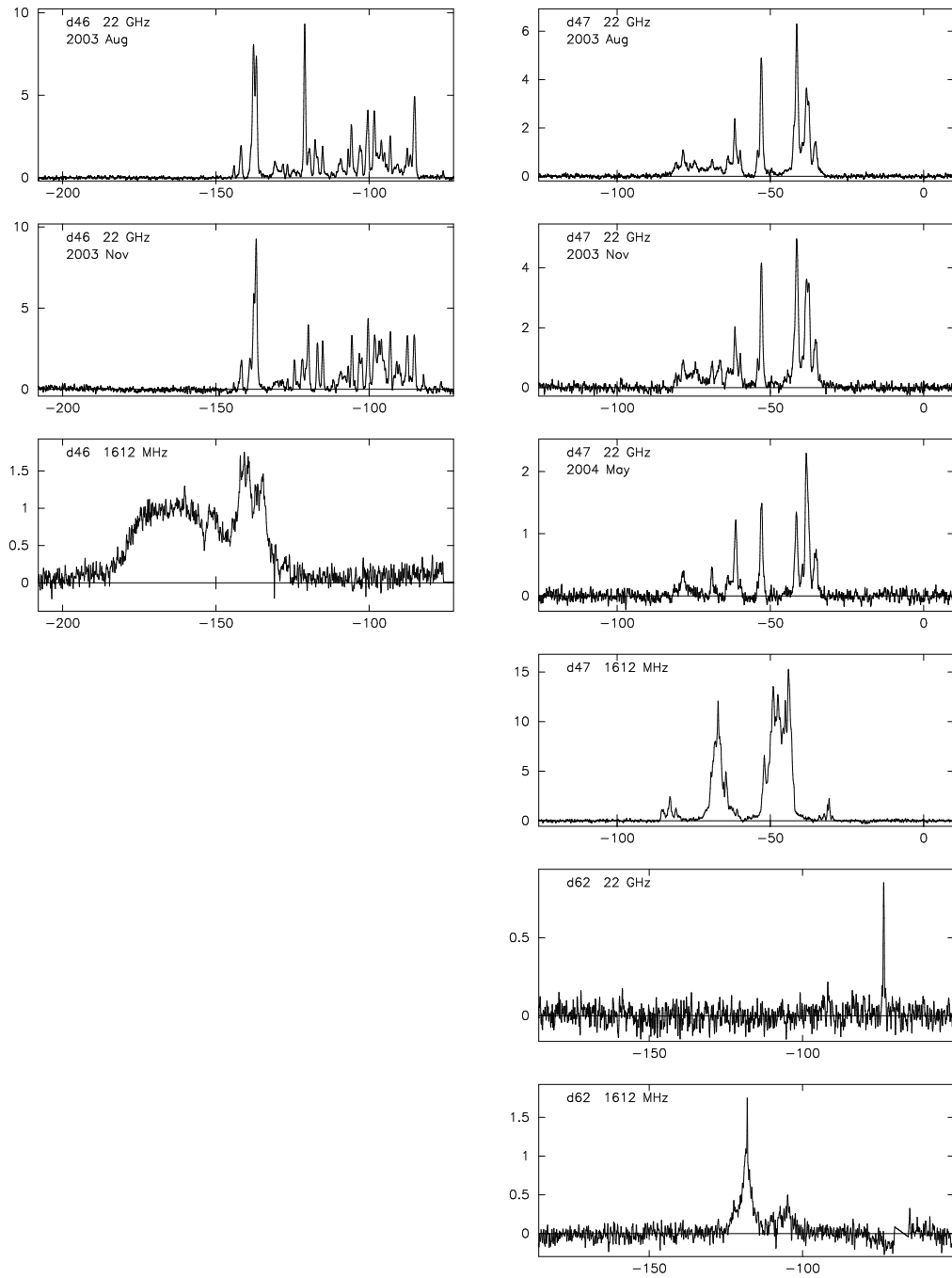


Fig. 2.— 22 GHz H₂O maser spectra from Tidbinbilla telescope observations. Source names are noted on individual spectra. For d46 and d47 the observing dates are also given. The OH 1612 MHz maser spectra from Paper I are plotted for all the sources, for comparison.

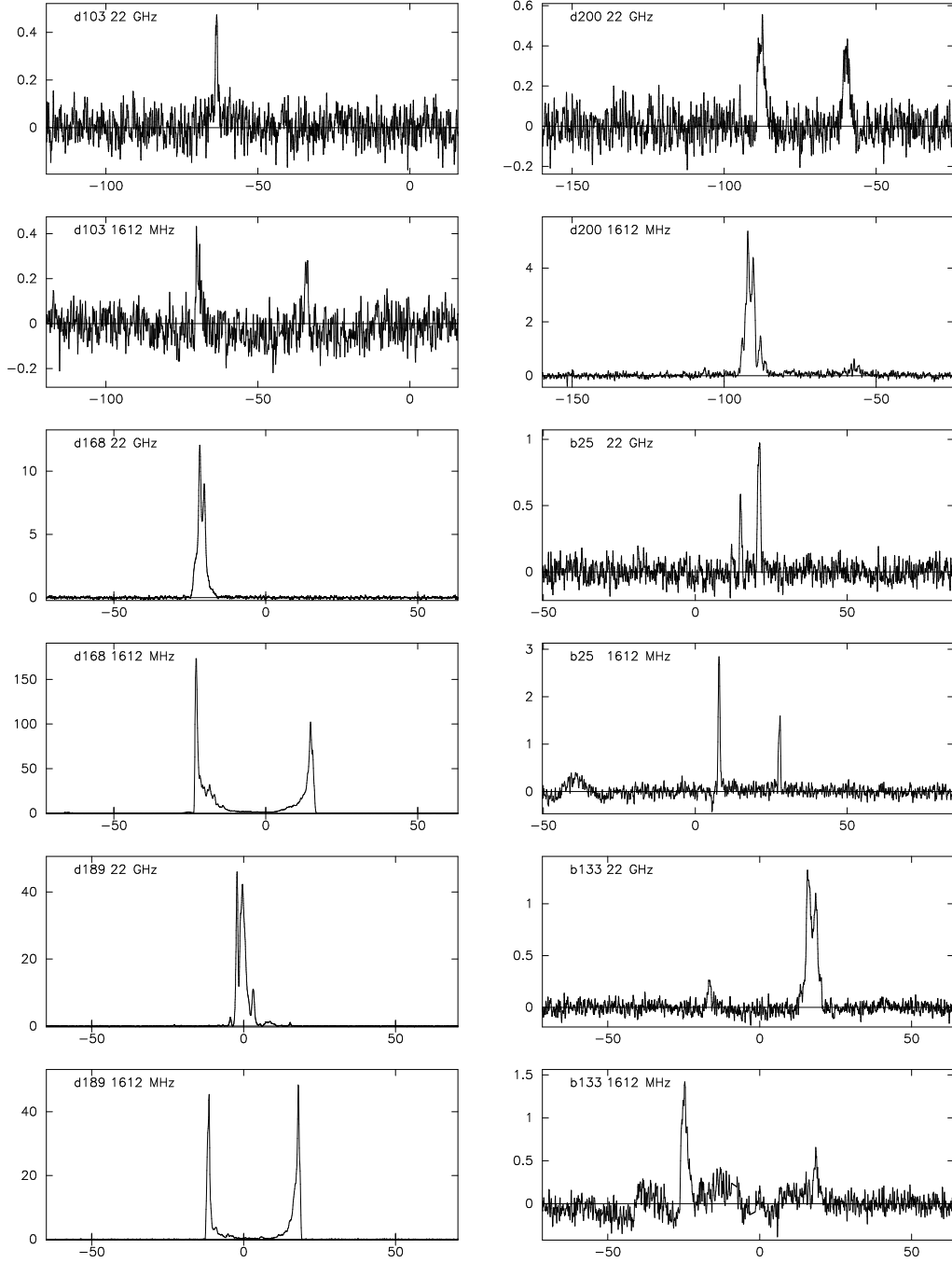


Fig. 3.— 22 GHz spectra continued.

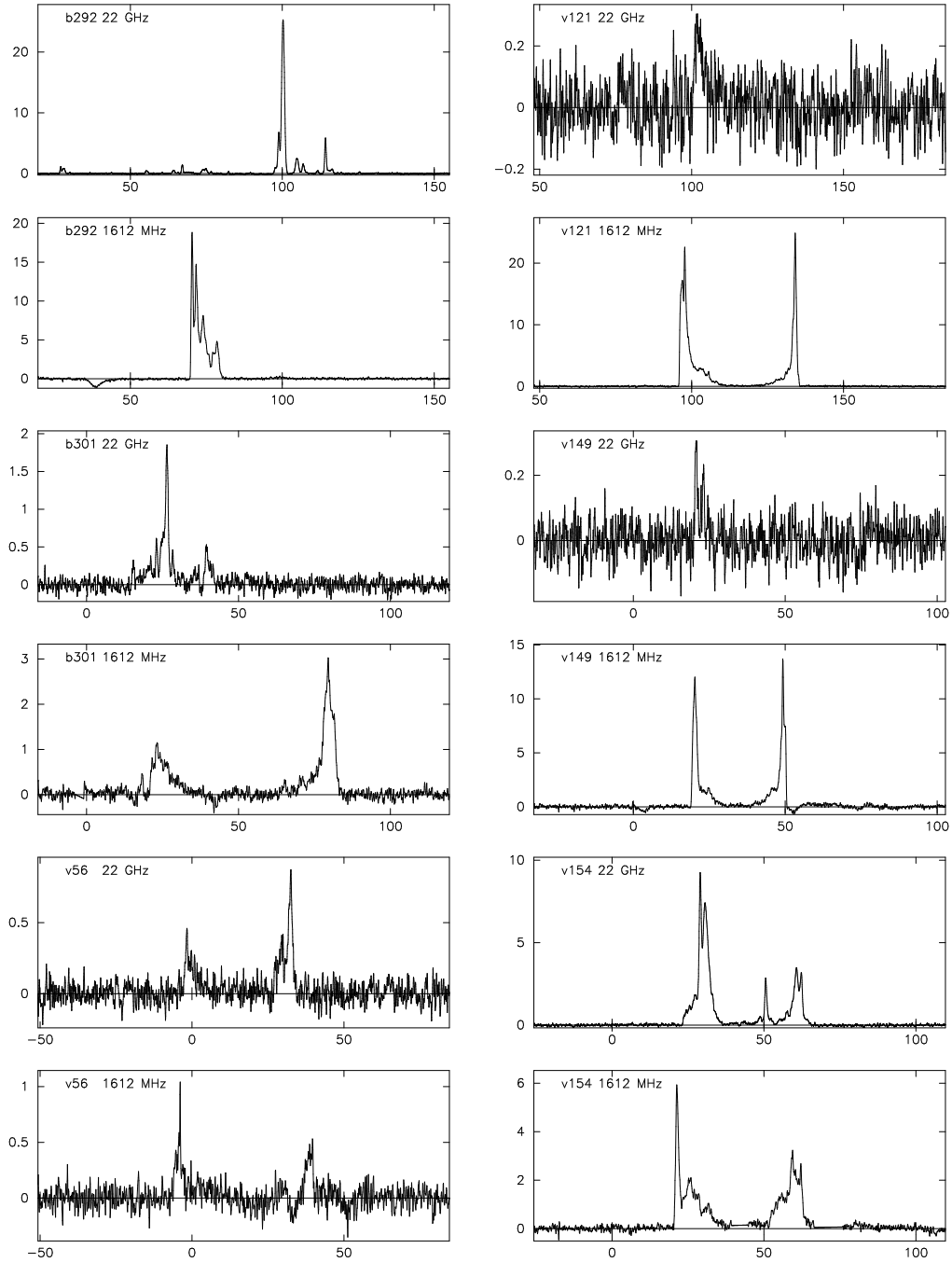


Fig. 4.— 22 GHz spectra continued. Note that for b292 the velocity range plotted does not cover the full extent of the maser emission (see Figure 6).

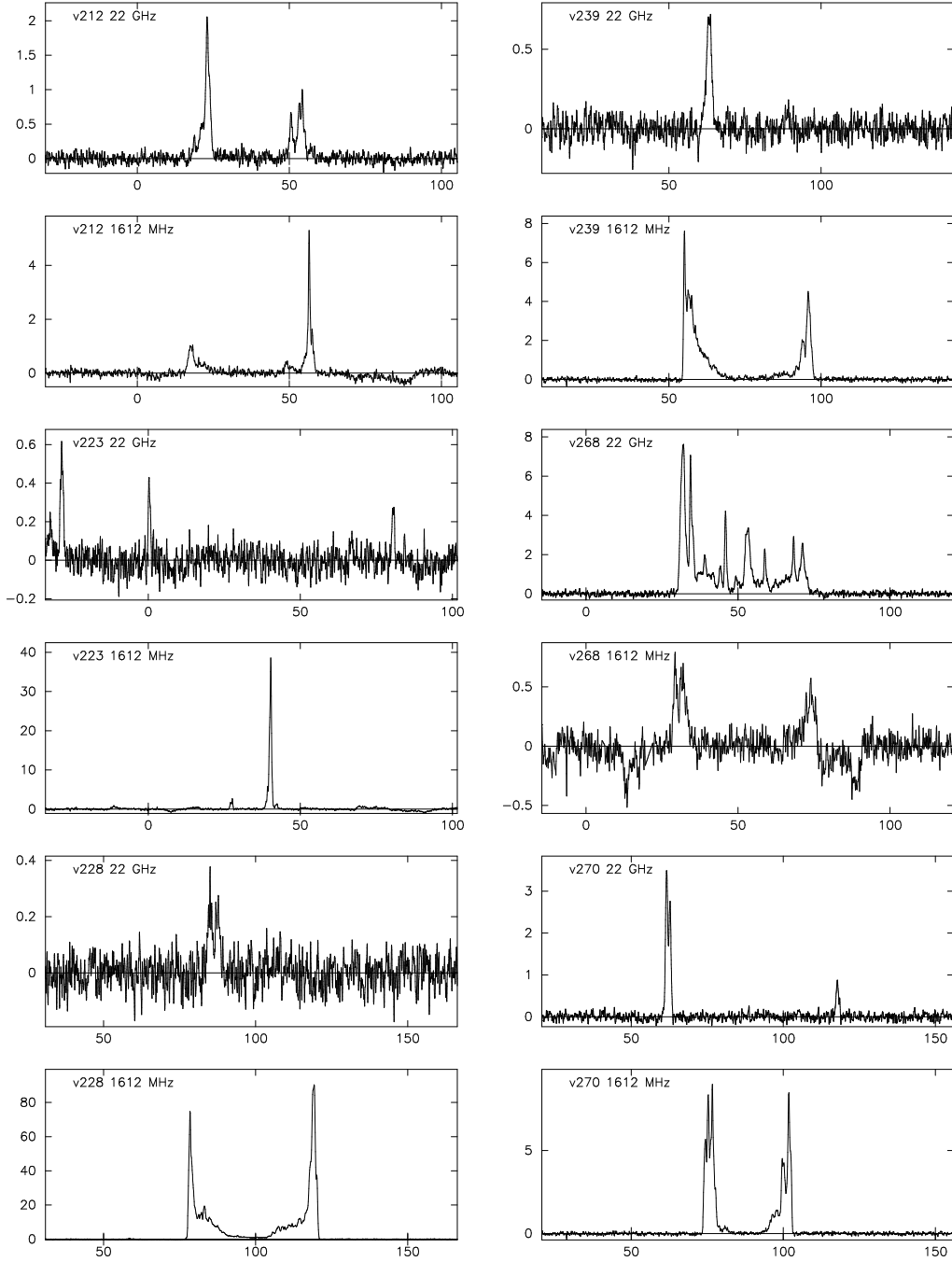


Fig. 5.— 22 GHz spectra continued. Note that for v223 the velocity range plotted does not cover the full extent of the maser emission (see Figure 6).

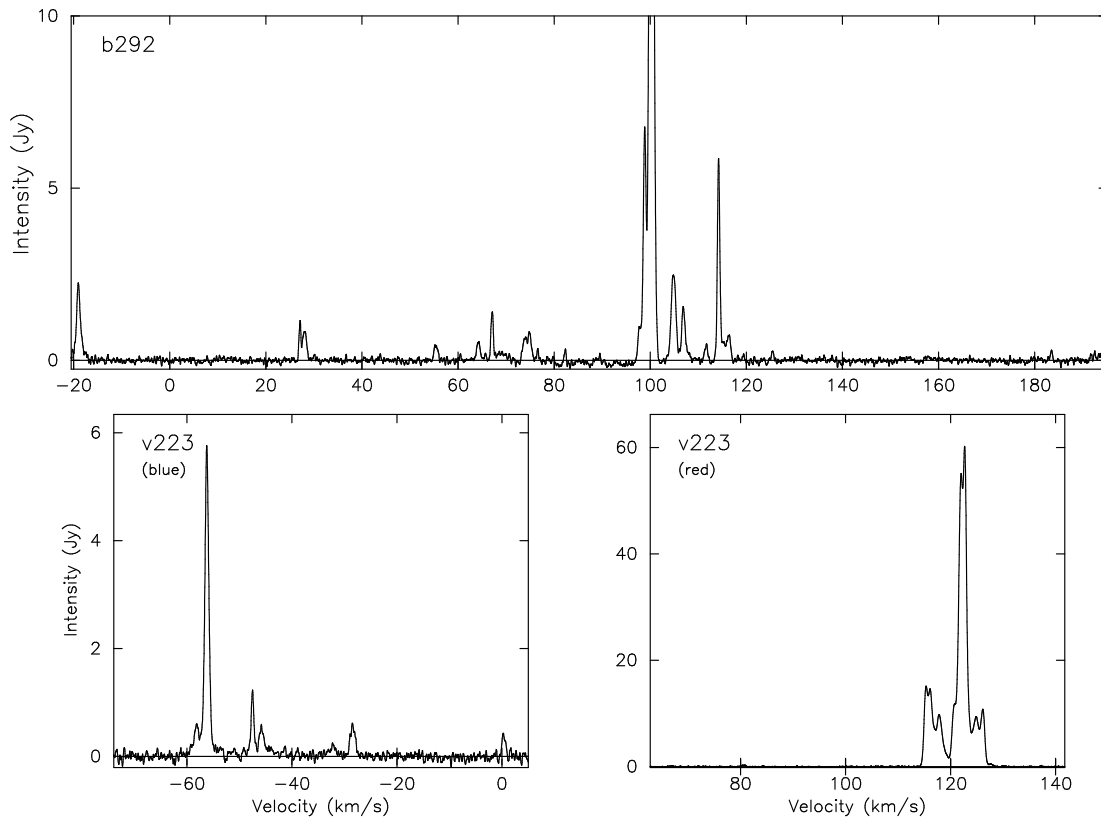


Fig. 6.— H_2O maser spectra for b292 and v223 showing the high velocity features. The *top* subfigure showing the spectrum for b292 over the entire observed velocity range. The stellar velocity is 87.3 km s^{-1} . The vertical axis is truncated to enable the weaker high-velocity features to be seen more easily. The full peak at 100 km s^{-1} can be seen in Figure 4. *Bottom*: The most blue-shifted (*left*) and red-shifted (*right*) features in the v223 spectra, on different vertical scales. The central velocity range of the v223 spectrum is shown in Figure 5. The stellar velocity is 33.9 km s^{-1} .

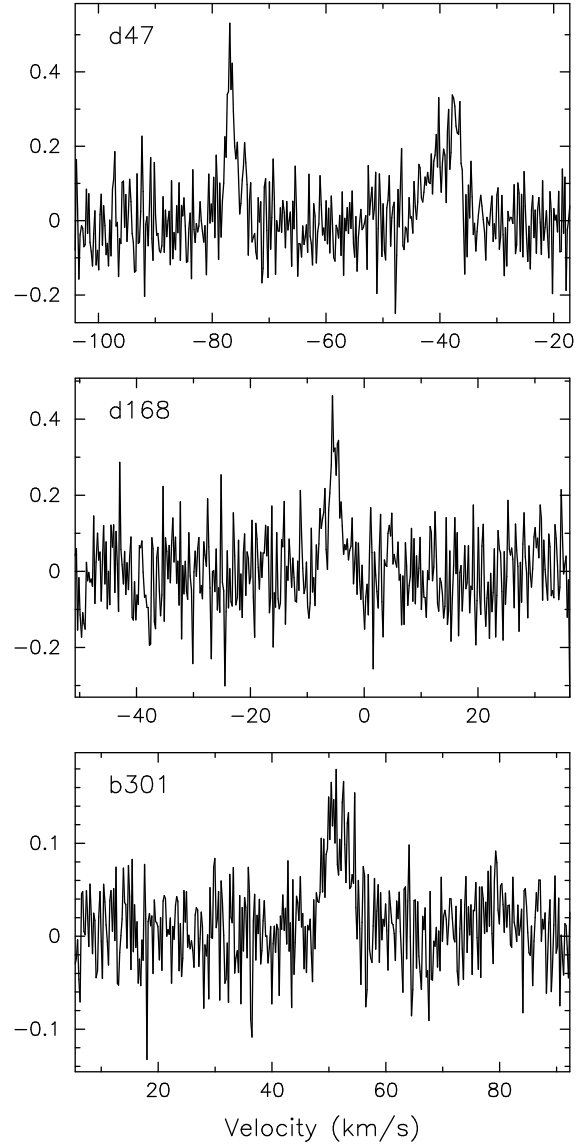


Fig. 7.— 86 GHz SiO maser profiles for d47, d168 and b301 measured using the Mopra radio telescope on 2004 August 26. The flux density scale is uncalibrated. Velocities are accurate to $\pm 1 \text{ km s}^{-1}$.

is very close in velocity to the OH emission from d59, but is probably not associated with d59 as this source is more than 8 arcmin away, substantially outside the Tidbinbilla beam. No other 22 GHz sources are reported near the stellar position and the source, though weak, was detected twice on 2003 November 15 and 2004 May 20 (the average spectrum is plotted). We infer that the H₂O maser emission is associated with d62.

d103: This source was detected twice (2004 February 28 and May 20). The averaged spectrum is plotted.

d168: Detected at both 22 GHz and 86 GHz. The SiO maser feature has a velocity of approximately -5 km s^{-1} , similar to the stellar velocity of -4.5 km s^{-1} (Deacon et al. 2004).

d189: The only source with a narrow H₂O maser emission profile centred on the stellar velocity determined from the OH 1612 MHz spectrum.

d200: Detected.

b17: Observed at 22 GHz (no detection) by Gómez et al. (1990).

b25: Narrow double-peaked spectrum with peaks located $\sim 7 \text{ km s}^{-1}$ inside the 1612 MHz peaks.

b70: Not detected. Observed at 22 GHz (no detection) by Likkell (1989) and at 86 GHz (no detection) by Nyman et al. (1998).

b96: Not detected. Observed at 22 GHz (no detection) by Gómez et al. (1990).

b128: Not detected. Observed at 86 GHz (no detection) by Nyman et al. (1998).

b133: Previously detected at 22 GHz by Taylor et al. (1993) with a similar, but weaker ($\sim 0.8 \text{ Jy}$), double-peaked spectrum.

b134: Not detected. Observed at 22 GHz (no detection) by Gómez et al. (1990) and at 86 GHz (no detection) by Nyman et al. (1998).

b143: Not detected. Observed at 86 GHz (no detection) by Nyman et al. (1998).

b251: Not detected. Observed at 22 GHz (no detection) by Gómez et al. (1990).

b292: This source has a very weak 1612 MHz peak near 100 km s^{-1} that is barely visible in Figure 4. Several blue- and red-shifted 22 GHz features are detected at velocities that are well outside the velocity range of the OH 1612 MHz emission (Figure 6). A weak red-shifted feature was detected at a velocity of 184 km s^{-1} near the edge of our bandpass and it is possible that other features may extend beyond the range of velocities observed. No known

H₂O maser sources are located near this source within the beam. We infer that the high-velocity features are associated with b292. This source is also the only known post-AGB star with OH 1720 MHz maser emission (Sevenster & Chapman 2001), and is discussed further in Section 6.2.

b301: Detected. Also detected at 22 GHz in 1987 by Valdetaro et al. (2001) but not detected by Takaba et al. (2001). 86 GHz SiO maser emission was detected at Mopra, with one feature at approximately 50 km s⁻¹.

v45: Not detected. Observed at 22 GHz (no detection) by Gómez et al. (1990).

v56: Detected.

v67: Not detected. Detected at 22 GHz (Gómez et al. 1990; Benson & Little-Marenin 1996; Valdetaro et al. 2001). In a 10 year monitoring program by Engels (2002), the H₂O emission was strongest in 1992 (4 Jy) but faded and was undetected after 1997. There was no detection by Takaba et al. (2001). Detected at 43 GHz by Gómez et al. (1990) but not by Nyman et al. (1998). Observed 86 GHz (no detection) by Nyman et al. (1998).

v87: Not detected. Detected at 22 GHz (1990) by Valdetaro et al. (2001) but no detection in Takaba et al. (1994).

v117: Not detected. Observed at 22 GHz (no detection) by Gómez et al. (1990).

v121: Marginal detection. Not detected by Takaba et al. (2001). Detected at SiO 43 GHz with no 86 GHz detection (Gómez et al. 1990; Nyman et al. 1998).

v132: Not detected. Detected at 22 GHz by Nyman, Johansson & Booth (1986) and Likkell (1989); this source was a ≥ 50 Jy H₂O maser source in the 1980's. It was monitored for 10 years by Engels (2002), growing weaker and finally disappearing after 1990 (Engels 2002; Takaba et al. 2001). Observed at 86 GHz (no detection) by Nyman et al. (1998)

v149: Observed twice, on 2004 February 28 and May 20. The averaged spectrum is plotted.

v154: The blue-shifted peak was detected by Gómez et al. (1990), Takaba et al. (1994), Takaba et al. (2001) and Valdetaro et al. (2001), with the most red-shifted peak faint or undetected. Detected at 43 GHz (Gómez et al. 1990).

v162: Not detected. Observed at 22 GHz (no detection) by Benson & Little-Marenin (1996).

v169: Not detected. Observed at 22 GHz (no detection) by Gómez et al. (1990).

v172: Not detected. Observed at 22 GHz (no detection) by Gómez et al. (1990).

v204: Not detected. Observed at 22 GHz (no detection) by Gómez et al. (1990).

v211: Not detected. Detected at 22 and 43 GHz by Gómez et al. (1990). Observed at 22 GHz (no detection) by Nyman, Johansson & Booth (1986).

v212: Detected.

v223: Extreme blue- and red-shifted features are present. This star has been imaged previously at OH (1612 MHz), H₂O (22 GHz) and SiO (43 GHz) maser frequencies (Imai et al. 2002, 2005) confirming the object as a post-AGB source with high-velocity H₂O jets located outside the shell of OH masers. The H₂O maser spectrum is highly variable (Likkell et al. 1992). Observed at 86 GHz (no detection) by Nyman et al. (1998). Discussed further in Section 6.1.

v228: Detected. Also detected at 22 GHz by Gómez et al. (1990) and Valdetaro et al. (2001) and detected at SiO 43 GHz by Gómez et al. (1990) and Nyman et al. (1998) (no detection at 86 GHz).

v231: Not detected. Observed at 22 GHz (no detection) by Gómez et al. (1990).

v239: Detected.

v268: About eight times stronger at 22 GHz than at 1612 MHz.

v270: A double-peaked profile with each peak 15 km s⁻¹ outside the 1612 MHz maser peaks. Previously detected at 22 GHz by Engels (2002), Gómez et al. (1994), Takaba et al. (2001) and Valdetaro et al. (2001). The fainter red-shifted peak is not always detected (e.g. Gómez et al. 1994), but there have been no other significant changes in the spectrum. Observed at 86 GHz (no detection) by Nyman et al. (1998). Discussed further in Section 6.2.

v274: Not detected. Observed at 22 GHz (no detection) by Likkell (1989).

5. SAMPLE ANALYSIS

5.1. Profile Types and IR colours

Of the 21 H₂O detections, 16 have available IRAS colours: 15 of these are LI sources and one is an RI source. Six sources have MSX colours with five identified as Quad IV (young post-AGB) and one as Quad I (older post-AGB).

Twelve sources have regular (R) H₂O maser spectra (Tables 3 and 4), with velocity widths equal to or slightly smaller (by 5 to 10 km s⁻¹) than their OH spectra, and either single- or double-peaked profiles. Single-peaked regular spectra have features at velocities located near the outer blue- or red-shifted OH emission peaks. The profiles of these sources indicate that the H₂O masers are located in regions of their circumstellar envelopes where the velocity gradients are small and radial amplification dominates, as for the OH 1612 MHz masers in many OH/IR sources. As noted in previous studies, blue-shifted features tend to be brighter than the red-shifted features. Of the 12 sources with regular profiles, eight have strongest emission at blue-shifted velocities while four have strongest emission at red-shifted velocities.

Five high-velocity sources (d46, b292, v223, d62 and v270) were detected. For each of these the velocity range of the H₂O maser emission is broader than that of the OH. The detection of these sources provides strong evidence for a ‘turn-on’ of high-velocity outflows in the lower mass post-AGB stars. It is remarkable that for four of the five sources the H₂O maser emission is strongest on the *red-shifted* side, in contrast to the sources with regular profiles. We are unable to explain this difference. The high-velocity H₂O maser sources are discussed further in Section 6.1.

Three LI sources (d47, v154 and v268) have irregular spectra with many emission features over their profiles. These sources clearly have complex masing regions, probably with a combination of tangential and radial amplification. For each of these the velocity range of the H₂O maser emission lies within that of the OH maser emission.

For 16 of the 21 candidate post-AGB stars, the peak H₂O maser flux density is weaker than the peak OH 1612 MHz maser flux density. Five sources (d46, b292, v154, v223 and v268) have stronger H₂O masers. These include three of the five high-velocity sources (d46, b292 and v223) and two LI sources with irregular spectra (v154 and v268).

Only one source, d189, has an S profile, with several closely-spaced features near the stellar velocity. This spectrum is similar to that of some Miras where the H₂O masers are located in a inner, accelerating region and so are tangentially amplified. With a red IRAS [12–25] colour of 1.2, it is unusual for d189 to have such a narrow Mira-like profile (Section 1). There is also evidence for an accelerating outflow in the OH mainline spectra of d189. A central plateau of emission is present in both the 1665 and 1667 MHz spectra (Paper I). Both mainline spectra also have features at velocities near the 1612 MHz peaks that probably arise from a remnant regular circumstellar envelope. The plateau mainline emission covers a similar velocity range to the H₂O maser emission.

There is no evidence in this study for an evolution from R to S profiles at IRAS [12–25]

≥ 0.5 as suggested by Engels (2002). In that work the detection of Mira-like S profiles from some post-AGB stars was considered to be due to decreasing mass-loss rates as stars evolved away from the AGB.

Figure 8 gives histograms for the source detections for IRAS [12–25] and MSX [8–12] colours, showing the drop in H₂O detection rates at redder colours. For 69 sources with available IRAS [12–25] colours, the detection rate is ~ 50 per cent for [12–25] < 1.3 . There is a clear drop in the detection rate at [12–25] ~ 1.3 , with only 2/40 sources detected at redder colours, and no detections for [12–25] > 1.9 . Similar results were found by Engels & Lewis (1996) and Takaba et al. (2001). For 57 sources with MSX colours, the detection rate is ~ 55 per cent for [8–12] < 0.6 with a sharp drop in the detection rate at [8–12] ~ 0.6 . However, a larger fraction of sources (7/38) were detected at redder colours. Five of these are high-velocity sources.

From our sample of 85 sources we find that the detection rates are consistent with a strong decrease in the H₂O maser emission from the circumstellar envelope as a star leaves the AGB. However, in some sources, a new source of strong H₂O maser emission turns on in the post-AGB phase with high-velocity outflows and/or irregular profiles. As discussed in Section 6, the detection of such H₂O maser spectra is likely, in at least some cases, to be associated with the emergence of collimated jets from the central star and the onset of morphological changes in the circumstellar envelopes as a star evolves away from the AGB.

5.2. H₂O and SiO Masers in LI Sources

Of the 21 sources detected, 15 are LI sources giving a 50 per cent detection rate for this subset. The LI sources have very different OH and H₂O maser characteristics to the rest of the sample. As discussed in Paper I, their OH 1612 MHz spectral profiles are almost all double peaked with higher than average envelope expansion velocities. The lack of OH mainline masers (Paper I) and the high detection rate (50 per cent) for H₂O maser emission indicates cooler, denser envelopes than for most other sources in the sample.

The OH and H₂O maser properties of LI sources are consistent with a classification as high-mass AGB stars with high mass-loss rates. In the inner envelopes, the gas densities are more favourable for H₂O masers than OH mainline emission while at larger radii the photo-dissociation of H₂O molecules leads to OH 1612 MHz maser emission. The double-peaked OH 1612 MHz spectral profiles show that the envelopes are still mostly spherical.

Few conclusions can be drawn from the small number of 86 GHz SiO maser observations conducted. However, the detection of SiO maser emission from three LI sources is consistent

with an evolutionary status as AGB stars. Most of the 43 GHz SiO maser detections of this sample from previous studies are also LI sources (Section 4.1; the exception is v223).

The wide double-peaked SiO maser profile found in d47 is unusual as very few SiO maser sources have double-peaked profiles. This source also has an unusual four-peaked 1612 MHz OH maser profile and biconal outflow (Paper I, Chapman 1988). Several geometries may explain the SiO maser profile: a very large circumstellar envelope from a massive star as in IRAS 19312+1950 (Section 1.2); a torus as in OH 231.8+4.2, or a biconal SiO maser outflow as in v223 (W43A) (Imai et al. 2005). Further observations of this unique source are needed to investigate these possibilities.

5.3. H₂O Maser Variability

Multiple observations of some of the sources enabled the variability of H₂O maser features to be assessed. Spectral features are stable in velocity over a time-scale of a few months, as shown by the profile constancy in the multiple observations of d46, d47 and the repeat detections of d62, d103 and v149. However, the peak intensity of individual features and the integrated spectral flux density vary dramatically. A lifetime for individual H₂O masers in evolved stars of 1–3 years (e.g. Elitzur 1992; Bains et al. 2003), with high variability and low or no saturation, is consistent with these results.

Table 4. Detection statistics for infrared groups and H₂O maser profile types

Frequency / Profile	Total	RI	LI	Quad I	Quad IV
OH 1612 MHz maser detections					
1612 MHz	85	38	30	21	15
22 GHz H ₂ O maser detections by profile					
Total	21	1	15	1	5
Regular (R)	12	0	11	0	1
Single (S)	1	0	0	0	1
Irregular (I)	3	0	3	0	0
High-velocity (H)	5	1	1	1	3

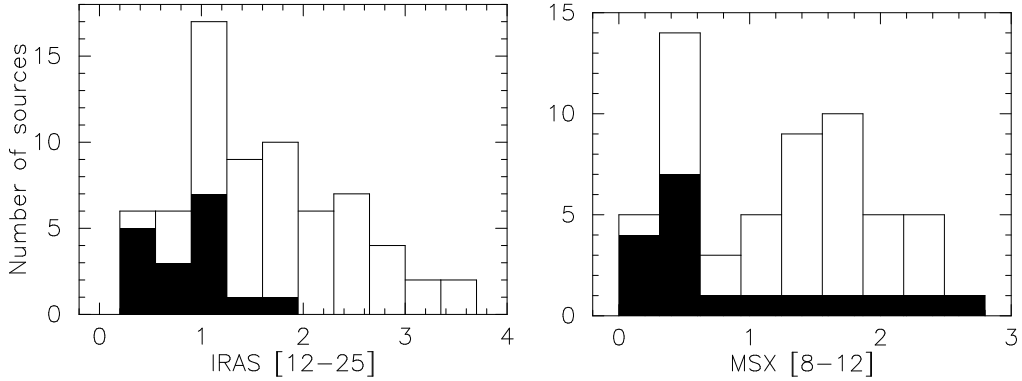


Fig. 8.— Two histograms of the number of sources observed (outline) and detected (filled) at 22 GHz versus IRAS [12–25] (*left*) and MSX [8–12] (*right*) colours. The overall detection rates were 25 per cent for the 69 sources with IRAS colours, and 32 per cent for the 57 sources with MSX colours.

6. DISCUSSION

6.1. High-Velocity and Water-Fountain H₂O Masers

We detected five sources with H₂O masers at velocities well outside their OH spectral range. Identifications for these sources are: v223 (W43A, IRAS18450–0148, OH 31.0+0.0), v270 (IRAS 18596+0315, OH 37.1–0.8), d46 (IRAS 15445–5449, OH 326.5–0.4), d62 (IRAS 15544-5332, OH 328.5–0.3) and b292 (IRAS 18043–2116, OH 0.9–0.4). Three sources, b292, v223 and v270, have MSX classifications as Quad IV sources (young post-AGB), one source, d46, is a MSX Quad I source (older post-AGB) while d62 is an IRAS LI source.

Two of the five sources, v223 and v270, have previously known H₂O maser emission. The source v223 (W43A) is well-known and belongs to a rare group of sources first described by Likkell & Morris (1988) as ‘water-fountains’. These are characterised by H₂O maser emission over an usually large velocity range. High resolution observations have revealed well-collimated bipolar jets. The H₂O masers are probably excited in post-shock regions as the expanding jets hit the ambient circumstellar material. In some cases the H₂O masers exhibit a strong degree of symmetry with pairs or groups of blue- and red-shifted emission features symmetrically placed on either side of the stellar position. The dynamical ages estimated for the jets are very short, typically around 100 years.

To date only four sources, v223 (W43A), IRAS 16342–3814 (OH 344.1+5.8), IRAS 19134+2131 and OH 12.8–0.9, are confirmed members of this class. The source v270 is also a likely water-fountain source although this has not yet been confirmed from high angular resolution observations. The properties of these five sources are briefly reviewed below:

v223 (W43A, IRAS 18450–0148, OH 31.0+0.0) Our spectrum of W43A from May 2004, plotted in Figures 5 and 6, shows strongest emission in two velocity ranges near 120 and –60 km s^{–1}, with strongest emission of 60 Jy at a red-shifted velocity of 122.7 km s^{–1}. Likkell et al. (1992) previously monitored the H₂O emission from 1987 to 1989. A comparison of their spectra shows the strongest emission over the same velocity ranges although the velocities of the strongest features are not the same. Strong emission at similar velocities was detected earlier by Genzel & Downes (1977) and Diamond et al. (1985). It thus appears that the velocity range of the stronger emission has remained stable over almost 30 years, although the individual emission features vary strongly. We note that the ratio of the strongest red-shifted emission to strongest blue-shifted emission was much larger in 2004 (10:1) than in the spectra taken approximately 15 years earlier (2:1). The Tidbinbilla spectrum also shows some additional weak features near –30, 0 and 80 km s^{–1} while the Likkell et al. data show additional features near 7 and 19 km s^{–1} that were not detected in

2004.

The high-velocity H₂O maser emission from v223 (W43A) occurs from two narrow jets on opposite sides of the central star, twice as far out as the OH masers (Imai et al. 2002, 2005) while emission at velocities close to the stellar velocity, is located inside the OH masers. Between 1994 and 2002 the separation between the most blue- and red-shifted H₂O maser clumps increased from 1700 to 2400 AU. A precessing jet model for the H₂O jets gives a dynamical age of only ~ 50 years, a precession period of 55 years, and a three-dimensional speed of 145 km s⁻¹ at an inclination of 39° with respect to the plane of the sky (Imai et al. 2005).

The H₂O masers in W43A are aligned along the jet axis. Recent polarisation observations have estimated the magnetic field strength in the jet to be 200 ± 75 milligauss (mG) and a toroidal configuration such that the field varies as r^{-1} where r is the radius from the star (Vlemmings et al. 2006). Extrapolating back to the stellar surface, this gives an equatorial magnetic field of 35 gauss (G) (if the jet H₂O masers are created in compressed, swept-up material) or 1.6 G (if the jet H₂O masers are created in shocks). The magnetic field strength and configuration suggests that the jet in v223 is magnetically collimated and is the most direct evidence thus far for magnetic collimation in evolved stars.

The OH 1612 MHz maser emission from W43A is double peaked with two clumps of masers separated on the sky and an OH expansion velocity of approximately 10 km s⁻¹. The blue-shifted OH masers and red-shifted H₂O masers are located on the NE side of the star and the red-shifted OH and blue-shifted H₂O masers on the SW side. This may be explained if the OH masers are located in an equatorial plane perpendicular to the H₂O jet. The dynamical age of the OH masers is ~ 2600 years (Imai et al. 2002).

W43A also has remarkable 43 GHz SiO maser emission. The SiO masers were imaged with the VLA and show a biconical outflow that is parallel to the H₂O jet, lying inside the OH masers (Imai et al. 2005). The SiO masers could be excited by shocks in the region between the jet and the OH masers.

v270 (IRAS 18596+0315, OH 37.1–0.8) H₂O maser emission from v270 was first detected in 1984 (Engels et al. 1986), but was initially considered to be unrelated because the velocity was outside the range of the OH masers. Our 2004 May H₂O maser spectrum of v270, shown in Figure 5, shows two narrow regions of emission, each approximately 30 km s⁻¹ from the stellar velocity, approximately twice the outflow velocity of the OH maser emission. Engels (2002) monitored the 22 GHz emission from v270 between 1990 and 1999 and identified nine spectral components with lifetimes for the individual components of

typically 2–3 years. Our more recent spectrum shows the same overall spectral structure although the individual components have changed.

VLA observations of v270 by Gómez et al. (1994) confirmed the coincidence of the OH and H₂O maser positions to within 1 arcsec. Later VLBA observations of the OH 1612 MHz masers found a bipolar morphology. The source is ~ 8 kpc away (Baud et al. 1985) and the red- and blue-shifted masers are in clumps that are separated by ~ 1300 AU (Gómez & Rodríguez 2000) probably indicating a bipolar outflow. The H₂O masers have not been imaged. From the symmetry of the source and the high-velocity H₂O features, we consider v270 to be a likely water-fountain source.

IRAS 16342–3814 (OH 344.1+5.8) This outflow source was first discovered by Likkell & Morris (1988) and te Lintel Hekkert et al. (1988) and shows high-velocity OH and H₂O masers. Hubble Space Telescope (HST) images show two asymmetric bipolar reflection lobes on either side of a dark lane. The OH masers are aligned with the inner edges of the lobes, with outflow velocities up to 70 km s^{-1} (Sahai et al. 1999; Zijlstra et al. 2001). Near-infrared images (Sahai et al. 2005) reveal corkscrew-like structures in the lobes which are consistent with a collimated precessing jet of diameter ≤ 100 AU and period ≤ 50 years.

H₂O maser emission from IRAS 16342–3814 is detected at radial velocities up to 160 km s^{-1} from the stellar velocity (Likkell & Morris 1988; Likkell et al. 1992; Morris et al. 2003). High angular resolution observations with the Very Long Baseline Array (VLBA, Morris et al. 2003; Claussen et al. 2004) have shown that these masers are located near the outer edges of the optical lobes close to the polar axis of the nebula. The red- and blue-shifted groups of H₂O maser spots show quasi-linear formations perpendicular to the nebula axis, consistent with bow shocks. For an estimated distance of 2 kpc this corresponds to a separation of 6000 AU, although Zijlstra et al. (2001) used a closer distance of 700 pc. The dynamical age of the jets is estimated to be 150 years (Claussen et al. 2004).

IRAS 19134+2131 This has two groups of H₂O maser features, separated by 100 km s^{-1} . There have been no detections of OH maser emission (Likkell et al. 1992). The H₂O maser emission also reveal bipolar jets, with a dynamical age of around 50 years old, although these are less collimated than for W43A (Imai et al. 2004). From measurements of the secular motion of the maser spots, a far kinematic distance of ≥ 16 kpc has been determined for this source (Imai et al. 2004).

OH 12.8–0.9 This is the most recently confirmed water-fountain source (Boboltz & Marvel 2005). It has a regular double-peaked OH 1612 MHz maser profile (24 km s^{-1} width) typical of an OH/IR star, and a H_2O maser profile that is also double-peaked but with a velocity width about twice as large (48 km s^{-1}). Similarly for IRAS 16342–3814, the H_2O masers occur in arcuate structures at the end of bipolar jets, with the blue- and red-shifted groups of masers separated by $\sim 110 \text{ mas}$. The jet opening angle is estimated to be 10° – 13° (Boboltz & Marvel 2005). The distance to OH 12.8–0.9 is uncertain, but assuming the source is close to the Galactic Centre with a distance of 8 kpc, the spatial separation on the sky of the clumps is about 870 AU. This gives an upper limit of 110 years on the dynamical age of the jets. The source has a lower outflow velocity and smaller jet length than other water-fountain sources, but its likely AGB/post-AGB status combined with the H_2O jet, firmly classify it as such.

6.2. A New Water-Fountain Source: b292

b292 (IRAS 18043–2116, OH 0.9–0.4) We report the discovery of a new water-fountain source, b292. H_2O maser emission from b292 was first detected from a ‘snapshot’ observation taken with the ATCA in 2002 (see Paper I). The velocity coverage of the 2002 observation was limited to velocities between approximately 65 and 110 km s^{-1} . Three maser features were detected at velocities of 73, 85 and 106 km s^{-1} .

Figure 6 shows the more recent spectrum, obtained in 2004 March with the Tidbinbilla telescope, with the much wider velocity coverage of approximately 210 km s^{-1} . This shows the discovery of many discrete features over velocities between -20 and 185 km s^{-1} . It is possible that even higher velocity features may exist outside this velocity range. The H_2O maser emission was detected within the 50 arcsec beam of the Tidbinbilla telescope and is almost certainly associated with the evolved star, which has a systemic velocity of 87 km s^{-1} .

A comparison of the ATCA and Tidbinbilla spectra for the inner velocity range shows that the maser emission is highly variable and may be rapidly increasing in strength. In the more recent spectrum, the H_2O maser emission was strongest at velocities between ~ 95 and 120 km s^{-1} corresponding to the red-shifted side (see below). The strongest emission peak has a flux density of 25 Jy at a velocity of 100 km s^{-1} . This feature was not detected in the spectrum obtained just 18 months earlier. No obvious pair symmetry is seen in the higher velocity extreme red- and blue-shifted features.

The OH maser properties of b292 have been previously discussed by Sevenster & Chapman

(2001) and in Paper I. The source is unusual in having emission at OH 1612 and 1665 MHz, but not at 1667 MHz. Both the 1612 and 1665 MHz emission extend over $\sim 33 \text{ km s}^{-1}$. It is also the only post-AGB star with detected OH 1720 MHz maser emission, although 1720 MHz emission has been recently detected in the PN K3–35 (Gómez et al. 2005), also an H₂O maser source. From Sevenster & Chapman (2001), 1720 MHz masers are produced behind a C-type shock under very specific physical conditions. The density increases behind the shock front, leading to the formation of H₂O molecules. Subsequent dissociation of the H₂O can then lead to the shock-excited OH emission at 1720 MHz. Sevenster & Chapman (2001) predicted that no H₂O maser emission would be detected from b292 as the density behind the shock front would not increase sufficiently for H₂O maser emission to occur. However, the new detection of high-velocity H₂O emission from b292 and the detection of OH 1720 MHz emission in K3–35 provides strong evidence that sufficiently high densities can occur.

Although no high resolution images have been obtained, it appears likely that both the OH 1720 MHz maser emission and the higher velocity H₂O maser features are associated with a high-velocity jet, with the H₂O maser emission located at greater distances. The OH 1612 and 1665 MHz masers are most likely associated with the remnant circumstellar envelope. It is unclear whether some H₂O maser features with velocities near the stellar velocity may still be present inside the OH radius.

From the extremely broad H₂O spectrum we identify b292 as highly likely to be a water-fountain source and note that the range of H₂O velocities, compared with the OH velocity range, is the most extreme known. High angular resolution and monitoring observations of this source would be valuable in confirming the proposed model.

6.3. Two High-Velocity Sources: d62 and d46

d62 (IRAS 15544–5332, OH328.5–0.3) This is classified as an LI source and so is likely to be from a massive progenitor star. The irregular OH spectrum is unusual for an LI source with 1612, 1665 and 1667 MHz emission detected at velocities between -100 and -130 km s^{-1} and the strongest integrated emission measured at OH 1667 MHz (Paper I). The OH spectra indicate a stellar velocity near -115 km s^{-1} although the velocity is not well determined.

The 22 GHz spectrum of d62, obtained from observations in November 2003 and May 2004, shows a single emission feature at a velocity of -74 km s^{-1} , offset by $\sim 40 \text{ km s}^{-1}$ from the central OH velocity (Figure 2). A corresponding blue-shifted peak (expected near -155 km s^{-1}) has not been detected. The single high-velocity red-shifted emission feature

suggests it is possible that d62 is a water-fountain source, although further observations are needed to clarify the classification.

d46 (IRAS 15445–5449, OH 326.5–0.4) The source d46 is highly unusual. It was first detected in 1994, in the OH transitions at 1612 MHz (Sevenster et al. 1997b) and 1665 MHz (Caswell 1998), and in 1998 at 1667 MHz (Sevenster & Chapman 2006, private communication). The OH profiles are all extremely wide, with emission velocities between -200 and -100 km s $^{-1}$. However, the OH 1667 MHz spectrum is blue-shifted relative to the OH 1612 MHz spectrum, while the OH 1665 MHz spectrum is slightly red-shifted. Figure 9 displays the OH emission from the three frequencies 1612, 1665 and 1667 MHz, and the 22 GHz H $_2$ O maser emission, overlaid to show the offsets between the lines. The H $_2$ O profile is red-shifted by approximately 50 km s $^{-1}$ relative to the OH profiles. The shape and width of the OH profiles are somewhat similar to those of some bipolar post-AGB high-velocity sources, including IRAS 18491–0207 and IRAS 11385–5517 (e.g. Zijlstra et al. 2001). However, the velocity shifts between the lines are exceptional. A comparison of several peak flux densities between 1994 and 2003 indicates that the OH maser emission is increasing in strength, with peak 1612 MHz flux densities of 0.8 Jy in 1994, 1.2 Jy in 1998 and 1.8 Jy in 2003.

Figures 2 and 9 show the OH 1612 MHz and H $_2$ O spectra for d46. The H $_2$ O spectrum has numerous narrow features blended together at velocities between -145 and -54 km s $^{-1}$. The two spectra taken in August and November 2003 show essentially the same spectral features, although with different peak flux densities. Given the different velocity ranges of the maser profiles, it is difficult to estimate the stellar velocity. However, it seems plausible to take a value close to the mid-point of the OH profiles, near a velocity of -150 km s $^{-1}$. This would mean that the high-velocity H $_2$ O masers have been produced at the back of the circumstellar envelope, perhaps from a one-sided jet-like structure.

From the radio continuum observations taken in November 1998, radio continuum was detected from d46 with Gaussian-fitted flux densities at 3, 6 and 13 cm of 11, 18 and 30 mJy respectively. These correspond to a steep non-thermal spectrum with a spectral index of -0.8 . With the limited u - v coverage of the ATCA observations, it was not possible to determine if the emission was spatially resolved.

As discussed by Cohen et al. (2006), nonthermal radio continuum emission with a spectral index of -0.8 is typical of Wolf-Rayet (WR) stars in binary systems, where synchrotron radio continuum emission occurs from the shocked regions at the interaction between the winds from two massive stars. For WR stars, the 6-cm radio continuum luminosity is typically 2×10^{19} erg s $^{-1}$. Nonthermal radio continuum has also been discovered from the PN

V1018 Sco with a 6-cm radio continuum luminosity of $4.4 \times 10^{19} \text{ erg s}^{-1}$ (Cohen et al. 2006). This remarkable source is a near-LI star (Figure 1) where an optical PN is seen around a still pulsating AGB star (Cohen et al. 2006). The radio luminosity in V1018 Sco is comparable to that of WR stars but the synchrotron emission is associated with the interface between a hot fast wind and the slow AGB wind. For d46, a kinematic distance of 7 kpc (calculated assuming a flat Galactic rotation model, a circular rotation speed of 220 km s^{-1} and a Galactic Centre distance of 8.5 kpc; e.g. Fish et al. 2003) combined with the 6-cm flux density of 18 mJy, produces an estimate for the 6-cm luminosity of $10^{21} \text{ erg s}^{-1}$, more than an order of magnitude higher than for V1018 Sco and higher than for most WR stars. For an assumed bandwidth of 10 GHz, the total radio luminosity is $\sim 10^{31} \text{ erg s}^{-1}$. By comparison with WR stars where the ratio of kinetic energy to radio luminosity is about $10^6:1$, this indicates an available kinetic energy, in the shock regions, of approximately $10^{37} \text{ erg s}^{-1}$.

The presence of high-velocity OH and H₂O masers and non-thermal radio continuum emission, together with the MSX classification of d46 as an older post-AGB star, are all consistent with its status as an evolved post-AGB star with a highly disturbed envelope, where a fast wind has ploughed into the slow AGB wind creating strong shocks and generating synchrotron radio continuum and the H₂O masers. High resolution observations are needed to determine the structure of this extraordinary source.

6.4. Jet Origins

As discussed above, there are now eight high-velocity H₂O maser sources associated with evolved stars. For seven of them OH maser emission is also detected. From the OH and H₂O maser properties and their far infrared colours, four sources (W43A, IRAS 19134+2134, v270 and b292) are likely to be younger post-AGB stars. Two sources (IRAS 16342-3814 and d46) have extremely red far-infrared colours and broad OH emission and are older post-AGB stars, and two sources (d62 and OH12.8–0.9) are probably high-mass AGB stars. The observations are consistent with a scenario where a high-velocity wind is generated as a star leaves the AGB. The detection of two high-velocity sources in the LI stars suggests that for some massive stars the jets may turn on before the star has left the AGB. Initially the narrow collimated jets pierce through the circumstellar envelope, which is still largely spherical and may still have the classical double-peaked OH 1612 MHz spectral profiles. At a later stage the narrow jets may disappear but the bipolar lobes will become wider as the fast and slow winds continue to interact. In the ‘late’ post-AGB phase the remnant circumstellar envelope may appear highly disrupted with high-velocity bipolar flows also seen in OH.

The origin of high-velocity collimated jets in post-AGB stars is not yet fully understood.

The ‘Generalised Interacting Stellar Winds’ model (Kwok et al. 1978; Balick 1987), where a fast wind is shaped by a pre-existing asymmetry in the slow wind, can explain a broad range of envelope asymmetries, including bipolar and elliptical outflows. However, it does not provide an explanation for the high wind momentum, the highly-collimated jets seen in the water-fountain sources, or the point and multi-polar symmetry of some PN (e.g. Bujarrabal et al. 2001; Frank & Blackman 2004).

Recent observations and theoretical models suggest that the collimated jets are shaped by stellar magnetic fields. From VLBA observations Vlemmings et al. (2006) have measured strong linear and circular polarisation in the H₂O maser features of W43A, at distances up to 1000 AU from the central star. From the estimated field strengths they argue that the magnetic field is collimating the jet. Greaves (2002) has detected a toroidal magnetic field around the PN NGC 7027.

Theoretical models show that strong magnetic fields may originate either in isolated stars (e.g. Matt et al. 2000), or as a result of close binary systems (e.g. Hollis & Koupelis 2000; Balick & Frank 2002). For single stars, the magnetic fields require a dynamo generated at the interface between a rapidly rotating stellar core and the more slowly rotating circumstellar envelope (Blackman et al. 2001). As the star sheds its outer layers and leaves the AGB, the core is increasingly exposed and, if the rotation speed is sufficiently high, the wind is strongly collimated by magneto-centrifugal forces. The magnetic field lines remove angular momentum from the core and magnetic braking then slows down the core rotation. This provides a natural explanation for the presence of strong collimation in the early post AGB stage, and also for the observed slow rotation rates of white dwarfs. ‘Magnetic explosions’ may also occur where energy is released from the wrapping of magnetic field lines that arise from the magnetised core (Matt et al. 2004). This mechanism may explain the ballistic outflows and multiple jet axes seen in many PPN.

Although the dynamo models are attractive there is some doubt that the dynamos can exist for long enough in post-AGB stars to influence the envelope morphology (e.g. Soker & Zoabi 2002). An alternative theory is that the collimated jets are driven out from the accretion disks of close binary systems, due to a combination of magnetic and centrifugal forces. In this scenario, momentum from the accretion disk is shed through the production of high-speed jets via an ordered magnetic field in the disk (Frank & Blackman 2004). The process is similar to jet formation from accretion disks around young stellar objects and active galactic nuclei. The accretion disk may be formed from the AGB wind of the primary around a compact secondary companion, or around the primary from the destruction of the secondary in common envelope evolution.

The incidence of binarity in post-AGB stars is likely to be ~ 50 per cent (e.g. de Ruyter et al.

2006; Zijlstra 2006). From a solar neighbourhood sample of 164 stars, Duquennoy & Mayor (1991) estimated that ~ 30 per cent of solar-type stars are isolated, with no companions above $0.01 M_{\odot}$. For their sample the median binary period was 180 years, corresponding to a binary separation of 35 AU.

Binary systems in post-AGB stars are hard to detect as the central stars are still surrounded by dust. One possible detection method, through radial velocity variations, is problematic because the orbital periods are mostly large enough to require monitoring for at least several years. In addition, the two central objects must be sufficiently close for mass transfer to occur if an accretion disk is to form. Mastrodemos & Morris (1999) have estimated that binary separations closer than about 24 AU are needed for an accretion disk to form. Given a median binary separation of 35 AU and a binary fraction of 1/2, possibly 10–15 per cent of post-AGB stars may be in close binary systems. Although this is hard to determine with any accuracy, it does appear that the fraction of evolved stars in close binary systems is too small to explain the high percentage of PN with aspherical geometries (e.g. Kwok 2000).

For AGB and post-AGB stars with detected maser emission, the incidence of close binary systems is expected to be small since the masers are likely to be highly disrupted in such systems. Of the 16 known binary post-AGB stars in de Ruyter et al. (2006), only two objects have OH maser emission. In searches for OH 1612 MHz maser emission from samples of symbiotic stars (Norris et al. 1984; Seaquist, Ivison, & Hall 1995, sample sizes 16 and 24 respectively) there were only two detections, both from systems thought to be relatively wide binaries. Schwarz et al. (1995) argue that binaries between 10 and 50 AU will not support OH masers, while those within 10 AU will not support any maser emission. Thus the presence of OH emission in particular, will favour single-star or wide-binary systems. Larger binary systems may show OH masers but would not be expected to form the accretion disks required to power the jets.

From the detections of OH masers as well as the high-velocity H_2O emission we consider that while binary systems may be responsible for the complex structures seen in some PN, the known water-fountain sources are unlikely to be in close binary systems. The jets may form from the dynamos associated with the single central stars. This would imply that dynamos generated in isolated stars can survive for long enough to support the observed jets. We note that our sources are from an OH-selected sample and thus is biased against high-velocity H_2O sources without OH emission. Only one high-velocity H_2O source without OH emission is currently known (IRAS 1934+2134).

7. CONCLUSIONS

- We have searched for 22 GHz H₂O maser emission from a well-defined sample of 85 candidate post-AGB stars. Twenty-one sources were detected. Of these detections, 12 had ‘regular’ (R) profiles similar to those seen in AGB stars. Five had high-velocity (H) profiles, three were classified as irregular (I) and one has a narrow velocity range near the stellar velocity (S).
- Fifteen of the H₂O maser detections were from the LI sources. The OH and H₂O maser properties of LI sources are consistent with their status as massive AGB stars with high mass-loss rates.
- High-velocity H₂O maser emission, with H₂O maser features detected outside of the velocity range of the OH emission, was detected from five sources. Two of these, v223 (W43A) and v270 (IRAS 19134+2134), have previously been identified. Three sources, d46, b292 and d62 are new discoveries. The source b292 is highly likely to be a water-fountain source. The source d46 is highly unusual and may be a more evolved water-fountain source. The status of d62 is less certain as only one emission feature was detected.
- For IRAS colours with $[12-25] > 1.3$ and MSX colours $[8-12] > 0.6$, the H₂O maser detection rate decreases strongly. Almost all sources detected with very red IRAS or MSX colours have high velocity or irregular outflows.
- From this survey of 85 sources, we surmise that the H₂O emission seen from AGB stars disappears as a star leaves the AGB. However, a new source of strong H₂O maser emission may appear which is associated with the emergence of collimated jets from the central star.
- We consider that the collimated jets seen in water-fountain sources are likely to be magnetically collimated from the dynamo action that occurs at the interface of the rapidly rotating stellar core and more slowly rotating circumstellar envelope and argue it is unlikely that the sources with both OH and H₂O masers are in close binary systems.
- SiO observations of 11 sources produced three detections, all from LI stars. One 86 GHz SiO maser source, d47, has an unusual very wide double-peaked SiO maser profile that may indicate there is a biconical outflow or torus around this star.

8. ACKNOWLEDGMENTS

We thank the referee of the paper, Mark Claussen, for his constructive and helpful comments on the manuscript, and Jim Lovell for taking all of the 22 GHz observations with the Tidbinbilla DSS–43 radio telescope. The Deep Space Network DSS–43 antenna is managed by the Jet Propulsion Laboratory, California Institute of Technology, under a contract with the National Aeronautics and Space Administration. Access for radio astronomy is provided through an agreement between the Australian and US governments and is coordinated by the Australia Telescope National Facility.

The Mopra radio telescope is part of the Australia Telescope which is funded by the Commonwealth of Australia for operation as a National Facility managed by CSIRO.

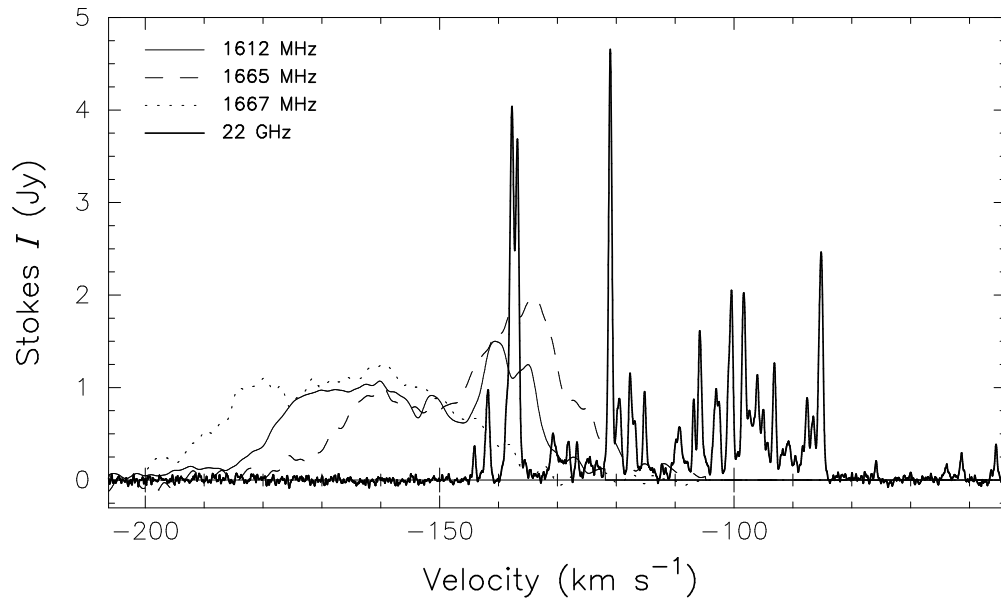


Fig. 9.— The OH 1612, 1665, 1667 MHz and 22 GHz H₂O maser emission from d46, with profiles plotted using the key given. The OH data are from Paper I but Gaussian-smoothed for clarity. The H₂O maser emission is from the 2003 August observation and is scaled by 0.5.

REFERENCES

- Bains, I., Cohen, R. J., Louridas, A., Richards, A. M. S., Rosa-González, D., & Yates, J. A. 2003, *MNRAS*, 342, 8
- Balick, B. 1987, *AJ*, 94, 671
- Balick, B., & Frank, A. 2002, *ARA&A*, 40, 439
- Baud, B., Sargent, A. I., Werner, M. W., & Bentley, A. F. 1985, *ApJ*, 292, 628
- Benson, P. J., & Little-Marenin, I. R. 1996, *ApJS*, 106, 579
- Blackman, E. G., Frank, A., Markiel, J. A., Thomas, J. H., & Van Horn, H. M. 2001, *Nature*, 409, 485
- Boboltz, D. A., & Marvel, K. B. 2005, *ApJ*, 627, L45
- Bujarrabal, V., Castro-Carrizo, A., Alcolea, J., & Sánchez Contreras, C. 2001, *A&A*, 377, 868
- Caswell, J. 1998, *MNRAS*, 297, 215
- Chapman, J. M. 1988, *MNRAS*, 230, 415
- Chapman, J. M., Habing, H. J., & Killeen, N. E. B. 1995, in *ASP Conf. Ser. 83, Astrophysical Applications of Stellar Pulsations*, eds. R. S. Stobie & P. A. Whitelock (San Francisco: ASP), 113
- Claussen, M., Sahai, R., & Morris, M. 2004, in *ASP Conf. Ser. 313, Asymmetrical Planetary Nebulae III: Winds, Structure and the Thunderbird*, eds. M. Meixner, J. H. Kastner, B. Balick, & N. Soker (San Francisco: ASP), 331
- Cohen, R. J. 1989, *RPPh*, 52, 881
- Cohen, M., Chapman, J. M., Deacon, R. M., Sault, R. J., Parker, Q. A., & Green, A. J. 2006, *MNRAS*, 369, 189
- Cooke, B., & Elitzur, M. 1985, *ApJ*, 295, 175
- de Gregorio-Monsalvo, I., Gómez, Y., Anglada, G., Cesaroni, R., Miranda, L. F., Gómez, J. F., & Torrelles, J. M. 2004, *ApJ*, 601, 921
- de Ruyter, S., van Winckel, H., Maas, T., Lloyd Evans, T., Waters, L. B. F. M., & Dejonghe, H. 2006, *A&A*, 448, 641

- Deacon, R. M., Chapman, J. M., & Green, A. J. 2004, *ApJS*, 155, 595
- Diamond, P. J., & Kemball, A. J. 2003, *ApJ*, 599, 1372
- Diamond, P. J., Norris, R. P., Rowland, P. R., Booth, R. S., & Nyman, L.-A. 1985, *MNRAS*, 212, 1
- Duquennoy, A., & Mayor, M. 1991, *A&A*, 248, 485
- Elitzur, M. 1992, *Astronomical Masers* (Dordrecht, Netherlands: Kluwer Academic Publishers)
- Engels, D. 2002, *A&A*, 388, 252
- Engels, D., & Lewis, B. M. 1996, *A&AS*, 116, 117
- Engels, D., Schmid-Burgk, J., & Walmsley, C. M. 1986, *A&A*, 167, 129
- Engels, D., Winnberg, A., Walmsley, C. M., & Brand, J. 1997, *A&A*, 322, 291
- Fish, V. L., Reid, M. J., Argon, A. L., & Menten, K. M. 2003, *ApJ*, 596, 328
- Frank, A., & Blackman, E. G. 2004, *ApJ*, 614, 737
- Frank, A., & Mellema, G. 1994, *ApJ*, 430, 800
- García-Segura, G., Langer, N., Różyczka, M., & Franco, J. 1999, *ApJ*, 517, 767
- Genzel, R., & Downes, D. 1977, *A&AS*. 30, 145
- Gómez, Y., Moran, J. M., & Rodríguez, L. F. 1990, *Rev. Mexicana Astron. Astrofis.*, 20, 55
- Gómez, Y., & Rodríguez, L. F. 2000, in *ASP Conf. Ser. 199, Asymmetrical Planetary Nebulae II: From Origins to Microstructures*, eds. J. H. Kastner, N. Soker, & S. Rappaport (San Francisco: ASP), 75
- Gómez, Y., & Rodríguez, L. F. 2001, *ApJ*, 557, L109
- Gómez, Y., Rodríguez, L. F., Contreras, M. E., & Moran, J. M. 1994, *Rev. Mexicana Astron. Astrofis.*, 28, 97
- Gómez, Y., Tafoya, D., Anglada, G., Franco-Hernández, R., Torrelles, J. M., & Miranda, L. F. 2005, *Mem. Soc. Astron. Italiana*, 76, 472
- Greaves, J. S. 2002, *A&A*, 392, L1

- Habing, H. J. 1996, *A&A Rev.*, 7, 97
- Hollis, J. M., & Koupelis, T. 2000, *ApJ*, 528, 418
- Humphreys, E. M. L. 2002, in *IAU Symp. 206, Cosmic Masers: From Protostars to Black Holes*, eds. V. Migenes & M. J. Reid (San Francisco: ASP), 266
- Imai, H., Morris, M., Sahai, R., Hachisuka, K., & Azzollini F., J. R. 2004, *A&A*, 420, 265
- Imai, H., Nakashima, J.-I., Diamond, P. J., Miyazaki, A., & Deguchi, S. 2005, *ApJ*, 622, L125
- Imai, H., Obara, K., Diamond, P. J., Omodaka, T., & Sasao, T. 2002, *Nature*, 417, 829
- Kwok, S. 2000, *The Origin and Evolution of Planetary Nebulae*, (Cambridge: Cambridge University Press)
- Kwok, S., Purton, C. R., & Fitzgerald, P. M. 1978, *ApJ*, 219, L125
- Lane, A. P., Johnston, K. J., Spencer, J. H., Bowers, P. F., & Diamond, P. J. 1987, *ApJ*, 323, 756
- Likkell, L. 1989, *ApJ*, 344, 350
- Likkell, L., & Morris, M. 1988, *ApJ*, 329, 914
- Likkell, L., Morris, M., & Maddalena, R. J. 1992, *A&A*, 256, 581
- Manchado, A., Villaver, E., Stanghellini, L., & Guerrero, M. A. 2000, in *ASP Conf. Ser. 199, Asymmetrical Planetary Nebulae II: From Origins to Microstructures*, eds. J. H. Kastner, N. Soker, & S. Rappaport (San Francisco: ASP), 17
- Mastrodemos, N., & Morris, M. 1999, *ApJ*, 523, 357
- Matt, S., Balick, B., Winglee, R., & Goodson, A. 2000, *ApJ*, 545, 965
- Matt, S., Frank, A., & Blackman, E. G. 2004, in *ASP Conf. Ser. 313, Asymmetrical Planetary Nebulae III*, eds. M. Meixner, J. H. Kastner, B. Balick, & N. Soker (San Francisco: ASP), 449
- Menten, K. M., & Melnick, G. J. 1991, *ApJ*, 377, 647
- Miranda, L. F., Gómez, Y., Anglada, G., & Torrelles, J. M. 2001, *Nature*, 414, 284

- Moran, J. M., Papadopoulos, G. D., Burke, B. F., Lo, K. Y., Schwartz, P. R., & Thacker, D. L. 1973, *ApJ*, 185, 535
- Morris, M. R., Sahai, R., & Claussen, M. 2003, in *Rev. Mexicana Astron. Astrofis. Conf. Ser. 15, Winds, Bubbles, and Explosions*, eds. S. J. Arthur & W. J. Henney (Mexico City: National Autonomous University of Mexico), 20
- Nakashima, J.-I., & Deguchi, S. 2000, *PASJ*, 52, L43
- Norris, R. P., Haynes, R. F., Wright, A. E., & Allen, D. A. 1984, *PASA*, 5, 562
- Nyman, L.-Å., Hall, P. J., & Olofsson, H. 1998, *A&AS*, 127, 185
- Nyman, L.-Å., Johansson, L. E. B., & Booth, R. S. 1986, *A&A*, 160, 352
- Sahai, R., Le Mignant, D., Sánchez Contreras, C., Campbell, R. D., & Chaffee, F. H. 2005, *ApJ*, 622, L53
- Sahai, R., te Lintel Hekkert, P., Morris, M., Zijlstra, A., & Likkell, L. 1999, *ApJ*, 514, L115
- Sahai, R., & Trauger, J. T. 1998, *AJ*, 116, 1357
- Sánchez Contreras, C., Desmurs, J. F., Bujarrabal, V., Alcolea, J., & Colomer, F. 2002, *A&A*, 385, L1
- Sault, R. J., Teuben, P. J., & Wright, M. C. H. 1995, in *ASP Conf. Ser. 77, Astronomical Data Analysis Software and Systems IV*, eds. R. A. Shaw, H. E. Payne, & J. J. E. Hayes (San Francisco: ASP), 433
- Schwarz, H. E., Nyman, L.-A., Seaquist, E. R., & Ivison, R. J. 1995, *A&A*, 303, 833
- Seaquist, E. R., Ivison, R. J., & Hall, P. J. 1995, *MNRAS*, 276, 867
- Sevenster, M. N. 2002a, *AJ*, 123, 2772
- Sevenster, M. N. 2002b, *AJ*, 123, 2788
- Sevenster, M. N., & Chapman, J. M. 2001, *ApJ*, 546, L119
- Sevenster, M. N., Chapman, J. M., Habing, H. J., Killeen, N. E. B., & Lindqvist, M. 1997a, *A&AS*, 122, 79
- Sevenster, M. N., Chapman, J. M., Habing, H. J., Killeen, N. E. B., & Lindqvist, M. 1997b, *A&AS*, 124, 509

- Sevenster, M. N., van Langevelde, H. J., Moody, R. A., Chapman, J. M., Habing, H. J., & Killeen, N. E. B. 2001, *A&A*, 366, 481
- Soker, N. 2001, *ApJ*, 558, 157
- Soker, N., & Zoabi, E. 2002, *MNRAS*, 329, 204
- Staveley-Smith, L. 1985, PhD thesis, University of Manchester
- Szymczak, M., & Engels, D. 1997, *A&A*, 322, 159
- Takaba, H., Iwate, T., Miyaji, T., & Deguchi, S. 2001, *PASJ*, 53, 517
- Takaba, H., Ukita, N., Miyaji, T., & Miyoshi, M. 1994, *PASJ*, 46, 629
- Taylor, G. B., Morris, M., & Schulman, E. 1993, *AJ*, 106, 1978
- te Lintel Hekkert, P., Habing, H. J., Caswell, J. L., Norris, R. P., & Haynes, R. F. 1988, *A&A*, 202, L19
- Valdettaro, R., et al 2001, *A&A*, 368, 845
- van der Veen, W. E. C. J., & Habing, H. J. 1988, *A&A*, 194, 125
- van der Veen, W. E. C. J., Habing, H. J., & Geballe, T. R. 1989, *A&A*, 226, 108
- van Hoof, P. A. M., Oudmaijer, R. D., & Waters, L. B. F. M. 1997, *MNRAS*, 289, 371
- Vassiliadis, E., & Wood, P. R. 1993, *ApJ*, 413, 641
- Vlemmings, W. H. T., Diamond, P. J., & Imai, H. 2006, *Nature*, 440, 58
- Wood, P. R. 2000, in *ASP Conf. Ser. 199, Asymmetrical Planetary Nebulae II: From Origins to Microstructures*, eds. J. H. Kastner, N. Soker, & S. Rappaport (San Francisco: ASP), 51
- Zijlstra, A. 2006, in *IAU Symp. 234, Planetary Nebulae in our Galaxy and Beyond*, eds. M. J. Barlow & R. H. Méndez (San Francisco: ASP), 55
- Zijlstra, A. A., Chapman, J. M., te Lintel Hekkert, P., Likkell, L., Comeron, F., Norris, R. P., Molster, F. J., & Cohen, R. J. 2001, *MNRAS*, 322, 280
- Zijlstra, A. A., Pottasch, S. R., Engels, D., Roelfsema, P. R., te Lintel Hekkert, P., & Umana, G. 1990, *MNRAS*, 246, 217